

Iterative Methods for Full-Scale Gaussian Process Approximations for Large Spatial Data

Tim Gyger^{†*} Reinhard Furrer[†] Fabio Sigrist^{*‡}

May 24, 2024

Abstract

Gaussian processes are flexible probabilistic regression models which are widely used in statistics and machine learning. However, a drawback is their limited scalability to large data sets. To alleviate this, we consider full-scale approximations (FSAs) that combine predictive process methods and covariance tapering, thus approximating both global and local structures. We show how iterative methods can be used to reduce the computational costs for calculating likelihoods, gradients, and predictive distributions with FSAs. We introduce a novel preconditioner and show that it accelerates the conjugate gradient method's convergence speed and mitigates its sensitivity with respect to the FSA parameters and the eigenvalue structure of the original covariance matrix, and we demonstrate empirically that it outperforms a state-of-the-art pivoted Cholesky preconditioner. Further, we present a novel, accurate, and fast way to calculate predictive variances relying on stochastic estimations and iterative methods. In both simulated and real-world data experiments, we find that our proposed methodology achieves the same accuracy as Cholesky-based computations with a substantial reduction in computational time. Finally, we also compare different approaches for determining inducing points in predictive process and FSA models. All methods are implemented in a free C++ software library with high-level Python and R packages (<https://github.com/fabsig/GPBoost>).

Keywords: Large data, spatial statistics, inducing point and predictive process approximation, conjugate gradient methods, stochastic Lanczos quadrature

*Institute of Financial Services Zug, Lucerne University of Applied Sciences and Arts (tim.gyger@hslu.ch)

[†]Department of Mathematical Modeling and Machine Learning, University of Zurich

[‡]Seminar for Statistics, ETH Zurich

1 Introduction

Gaussian process (GP) models are frequently used as probabilistic non-parametric models for spatial data. Calculating likelihoods and their gradients is typically done using a Cholesky factorization requiring $\mathcal{O}(n^3)$ operations and $\mathcal{O}(n^2)$ memory allocation, where n represents the number of observations. Computations for large data sets thus quickly become infeasible. A variety of strategies have been introduced to alleviate this computational burden; see, e.g., [Heaton et al. \[2019\]](#) for a review. Low-rank approximations such as predictive process models [\[Banerjee et al., 2008\]](#) and the Fully Independent Training Conditional (FITC) approximation [\[Quinero-Candela and Rasmussen, 2005\]](#), also known as modified predictive process approximation [\[Finley et al., 2009\]](#), have proven effective in modeling the large-scale structure of spatial processes. Another approach involves the use of sparse methods, where sparsity is enforced either on the precision matrices or the covariance matrices. A popular method to achieve sparsity in covariance matrices is covariance tapering, which sets the covariance to zero between two sufficiently distant locations [\[Furrer et al., 2006\]](#). Tapering is typically effective in capturing the short-scale structure of spatial processes and allows for using efficient sparse matrix algorithms. The computational complexity for factorizing a sparse $n \times n$ matrix is not linear in n but difficult to generalize since it depends on the corresponding graph and the fill-reducing ordering [\[Davis, 2006\]](#). We denote this computational complexity by $\mathcal{O}(g(n))$, where $g(\cdot)$ is a function of the sample size n . For instance, we have approximately $\mathcal{O}(n^{3/2})$ for two-dimensional spatial data and at least $\mathcal{O}(n^2)$ in higher dimensions [\[Lipton et al., 1979\]](#). The full-scale approximation (FSA) of [Sang and Huang \[2012\]](#) combines a low-rank approximation with tapering applied to a residual process thus capturing both long- and short-range correlations. For evaluating a log-likelihood, this approach involves the factorization of a sparse matrix resulting in $\mathcal{O}(n \cdot (m^2 + n_\gamma^2) + g(n))$ computational and $\mathcal{O}(n \cdot (m + n_\gamma))$ memory complexity when using a Cholesky decomposition, where n_γ is the average number of non-zero entries per row in the sparse matrix. Further, the computational complexity for calculating predictive variances is $\mathcal{O}(n \cdot n_p \cdot n_\gamma)$, where n_p denotes the number of prediction locations. I.e., both parameter estimation and prediction can become prohibitively slow for large n and n_p due to the above $n^{3/2}$ and $n \cdot n_p$ terms. Iterative numerical techniques [\[Trefethen and Bau, 2022\]](#) such as conjugate gradient (CG) algorithms and the Lanczos tridiagonalization algorithm, which require only matrix-vector multiplications that can be trivially parallelized, are an alternative to direct solver methods such as the Cholesky decomposition. Recently, a growing body of research [\[Aune et al., 2014, Gardner et al., 2018, Pleiss et al., 2018\]](#) has used these numerical approaches in combination with stochastic approximation methods such as the Hutchinson’s estimator [\[Hutchinson, 1989\]](#) and the stochastic Lanczos quadrature (SLQ) [\[Ubaru et al., 2017\]](#).

In this work, we propose iterative methods for likelihood evaluation, gradient calculation, and the computation of predictive distributions for full-scale approximations. We solve systems of linear equations using the CG method and can calculate the log determinant and its derivatives using SLQ and Hutchinson’s estimator, and we introduce a novel way to compute predictive variances through a combination of the CG method and stochastic diagonal estimation [\[Bekas et al., 2007\]](#). We also introduce a preconditioner that allows for further reducing run times and for doing variance reduction. We analyze our methods both theoretically and empirically on simulated and real-world

data. The remainder of the paper is organized as follows. Section 2 introduces the FSA. In Section 3, we introduce our iterative methodology for GP inference within the FSA framework. We discuss the advancements in computational efficiency and state convergence results for the CG method and its preconditioned variant. In Section 4, we conduct simulation studies to compare different inducing point methods and different combinations of approximation parameters m and γ . Furthermore, we analyze the computational efficiency and statistical properties of our methodology. In Section 5, we apply our methodology to a data set comprising daytime land surface temperatures in degrees Celsius.

2 Gaussian process models for spatial data sets

We assume the following GP model

$$\mathbf{Y} = F(\mathbf{X}) + \mathbf{b} + \boldsymbol{\epsilon}, \quad \mathbf{b} \sim \mathcal{N}(\mathbf{0}, \boldsymbol{\Sigma}), \quad \boldsymbol{\epsilon} \sim \mathcal{N}(\mathbf{0}, \sigma^2 \mathbf{I}_n), \quad (1)$$

where $\mathbf{Y} = (Y(\mathbf{s}_1), \dots, Y(\mathbf{s}_n))^T \in \mathbb{R}^n$ represents the response variable observed at locations $\mathcal{S} = \{\mathbf{s}_1, \dots, \mathbf{s}_n\}$, $\mathbf{s}_i \in \mathbb{R}^d$, and $F(\mathbf{X}) \in \mathbb{R}^n$ denotes the fixed effects. In the following, we assume $F(\mathbf{X}) = \mathbf{X}\boldsymbol{\beta}$, $\boldsymbol{\beta} \in \mathbb{R}^p$, $\mathbf{X} \in \mathbb{R}^{n \times p}$, but $F(\cdot)$ could also be modeled using machine learning methods such as tree-boosting [Sigrist, 2022a,b]. Further, $\boldsymbol{\epsilon} = (\epsilon(\mathbf{s}_1), \dots, \epsilon(\mathbf{s}_n))^T \in \mathbb{R}^n$ is an independent error term often referred to as the nugget effect. The zero-mean random effects $\mathbf{b} = (b(\mathbf{s}_1), \dots, b(\mathbf{s}_n))^T \in \mathbb{R}^n$ are a finite-dimensional version of a GP, and the covariance matrix is denoted as $\boldsymbol{\Sigma} \in \mathbb{R}^{n \times n}$, where its elements are determined by a covariance function $c(\cdot, \cdot)$

$$\Sigma_{ij} = \text{Cov}(b(\mathbf{s}_i), b(\mathbf{s}_j)) = c(\mathbf{s}_i, \mathbf{s}_j), \quad \mathbf{s}_i, \mathbf{s}_j \in \mathcal{S}.$$

The primary focus lies in the estimation of the regression coefficients denoted as $\boldsymbol{\beta}$ as well as the parameters characterizing the covariance matrix denoted by $\boldsymbol{\theta} \in \mathbb{R}^q$. For maximum likelihood estimation, we minimize the negative log-likelihood function

$$\mathcal{L}(\boldsymbol{\beta}, \boldsymbol{\theta}; \mathbf{y}, \mathbf{X}) = \frac{n}{2} \log(2\pi) + \frac{1}{2} \log \det(\tilde{\boldsymbol{\Sigma}}) + \frac{1}{2} (\mathbf{y} - \mathbf{X}\boldsymbol{\beta})^T \tilde{\boldsymbol{\Sigma}}^{-1} (\mathbf{y} - \mathbf{X}\boldsymbol{\beta}), \quad (2)$$

where $\tilde{\boldsymbol{\Sigma}} = \boldsymbol{\Sigma} + \sigma^2 \mathbf{I}_n$ is the covariance matrix of \mathbf{Y} and \mathbf{y} is the observed data. If a first- or second-order method for convex optimization such as the Broyden–Fletcher–Goldfarb–Shanno (BFGS) algorithm is used, the calculation of the gradient of the negative log-likelihood function with respect to the covariance parameters is required. The gradient is given by

$$\frac{\partial}{\partial \boldsymbol{\theta}} \mathcal{L}(\boldsymbol{\beta}, \boldsymbol{\theta}; \mathbf{y}, \mathbf{X}) = \frac{1}{2} \text{Tr} \left(\tilde{\boldsymbol{\Sigma}}^{-1} \frac{\partial \tilde{\boldsymbol{\Sigma}}}{\partial \boldsymbol{\theta}} \right) - \frac{1}{2} (\mathbf{y} - \mathbf{X}\boldsymbol{\beta})^T \tilde{\boldsymbol{\Sigma}}^{-1} \frac{\partial \tilde{\boldsymbol{\Sigma}}}{\partial \boldsymbol{\theta}} \tilde{\boldsymbol{\Sigma}}^{-1} (\mathbf{y} - \mathbf{X}\boldsymbol{\beta}). \quad (3)$$

The predictive distribution at n_p new locations $\mathcal{S}^p = \{\mathbf{s}_1^p, \dots, \mathbf{s}_{n_p}^p\}$ is $\mathcal{N}(\boldsymbol{\mu}^p, \boldsymbol{\Sigma}^p)$ with predictive mean $\boldsymbol{\mu}^p = \mathbf{X}^p \boldsymbol{\beta} + \boldsymbol{\Sigma}_{nn_p}^T \tilde{\boldsymbol{\Sigma}}^{-1} (\mathbf{y} - \mathbf{X}\boldsymbol{\beta})$ and predictive covariance $\boldsymbol{\Sigma}^p = \boldsymbol{\Sigma}_{n_p n_p} + \sigma^2 \mathbf{I}_{n_p} - \boldsymbol{\Sigma}_{nn_p}^T \tilde{\boldsymbol{\Sigma}}^{-1} \boldsymbol{\Sigma}_{nn_p} \in \mathbb{R}^{n_p \times n_p}$, where $\mathbf{X}_i^p = (X(\mathbf{s}_i^p)_1, \dots, X(\mathbf{s}_i^p)_p) \in \mathbb{R}^{1 \times p}$ is the i -th row of \mathbf{X}^p containing predictor variables for prediction i , $i = 1, \dots, n_p$, $\boldsymbol{\Sigma}_{nn_p} = [c(\mathbf{s}_i, \mathbf{s}_j^p)]_{i=1:n, j=1:n_p} \in \mathbb{R}^{n \times n_p}$ is a cross-covariance matrix, and $\boldsymbol{\Sigma}_{n_p} = [c(\mathbf{s}_i^p, \mathbf{s}_j^p)]_{i=1:n_p, j=1:n_p} \in \mathbb{R}^{n_p \times n_p}$.

2.1 Full-Scale approximation

The idea of the FSA [Sang and Huang, 2012] is to decompose the GP into two parts

$$\mathbf{b} = \mathbf{b}_l + \mathbf{b}_s,$$

where \mathbf{b}_l is a reduced rank predictive process modeling large-scale dependence and $\mathbf{b}_s = \mathbf{b} - \mathbf{b}_l$ is a residual process capturing the small-scale spatial dependence that is unexplained by the reduced rank process. For a fixed set $\mathcal{S}^* = \{\mathbf{s}_1^*, \dots, \mathbf{s}_m^*\}$ of m inducing points, or knots, the predictive process is given by

$$\mathbf{b}_l(\mathbf{s}_i) = c(\mathbf{s}_i, \mathcal{S}^*)^\top \Sigma_m^{-1} \mathbf{b}^*,$$

where $\mathbf{b}^* = (b(\mathbf{s}_1^*), \dots, b(\mathbf{s}_m^*))^\top$. Its finite rank covariance function is

$$c_l(\mathbf{s}_i, \mathbf{s}_j) = \text{Cov}(b_l(\mathbf{s}_i), b_l(\mathbf{s}_j)) = c(\mathbf{s}_i, \mathcal{S}^*)^\top \Sigma_m^{-1} c(\mathbf{s}_j, \mathcal{S}^*),$$

where $c(\mathbf{s}_i, \mathcal{S}^*) = (c(\mathbf{s}_i, \mathbf{s}_1^*), \dots, c(\mathbf{s}_i, \mathbf{s}_m^*))^\top$ and $\Sigma_m = [c(\mathbf{s}_i^*, \mathbf{s}_j^*)]_{i=1:m, j=1:m} \in \mathbb{R}^{m \times m}$ is a covariance matrix with respect to the inducing points. The corresponding covariance matrix is given by

$$\Sigma_l = \Sigma_m^\top \Sigma_m^{-1} \Sigma_{mn},$$

where $\Sigma_{mn} = [c(\mathbf{s}_i^*, \mathbf{s}_j)]_{i=1:m, j=1:n} \in \mathbb{R}^{m \times n}$ is a cross-covariance matrix between the inducing and data points. The covariance function of the residual process $\mathbf{b}_s(\mathbf{s})$ is

$$c(\mathbf{s}_i, \mathbf{s}_j) - c(\mathbf{s}_i, \mathcal{S}^*)^\top \Sigma_m^{-1} c(\mathbf{s}_j, \mathcal{S}^*).$$

In the FSA, this is approximated using tapering

$$c_s(\mathbf{s}_i, \mathbf{s}_j) = (c(\mathbf{s}_i, \mathbf{s}_j) - c(\mathbf{s}_i, \mathcal{S}^*)^\top \Sigma_m^{-1} c(\mathbf{s}_j, \mathcal{S}^*)) \cdot c_{\text{taper}}(\|\mathbf{s}_i - \mathbf{s}_j\|_2; \gamma),$$

where the tapering function $c_{\text{taper}}(\cdot; \gamma)$ is an isotropic correlation function which is zero for data located at any two positions whose distance exceeds the prescribed taper range parameter $\gamma > 0$, i.e., $c_{\text{taper}}(\|\mathbf{s}_i - \mathbf{s}_j\|_2; \gamma) = 0$ if $\|\mathbf{s}_i - \mathbf{s}_j\|_2 \geq \gamma$, for the Euclidean vector norm $\|\cdot\|_2$. The covariance matrix of the residual process is given by

$$\Sigma_s = (\Sigma - \Sigma_m^\top \Sigma_m^{-1} \Sigma_{mn}) \circ \mathbf{T}(\gamma),$$

where $\mathbf{T}(\gamma) = [c_{\text{taper}}(\|\mathbf{s}_i - \mathbf{s}_j\|_2; \gamma)]_{i=1:n, j=1:n}$ is the taper matrix, and the operator \circ refers to the elementwise matrix product also called the Hadamard product. The parameter γ determines the sparsity of the matrix Σ_s , and it controls a trade-off between accuracy and computational cost. In summary, the FSA of the original covariance function can be expressed as follows

$$c(\mathbf{s}_i, \mathbf{s}_j) \approx c_\dagger(\mathbf{s}_i, \mathbf{s}_j) = c_l(\mathbf{s}_i, \mathbf{s}_j) + c_s(\mathbf{s}_i, \mathbf{s}_j),$$

resulting in the covariance matrix approximation

$$\tilde{\Sigma}_\dagger = \Sigma_l + \Sigma_s + \sigma^2 \mathbf{I}_n \approx \tilde{\Sigma}.$$

2.2 Parameter estimation

For the full-scale approximation, the negative log-likelihood and its derivative are given by

$$\begin{aligned}\mathcal{L}_\dagger(\boldsymbol{\beta}, \boldsymbol{\theta}; \mathbf{y}, \mathbf{X}) &= \frac{n}{2} \log(2\pi) + \frac{1}{2} \log \det(\tilde{\boldsymbol{\Sigma}}_\dagger) + \frac{1}{2} (\mathbf{y} - \mathbf{X}\boldsymbol{\beta})^\top \tilde{\boldsymbol{\Sigma}}_\dagger^{-1} (\mathbf{y} - \mathbf{X}\boldsymbol{\beta}), \\ \frac{\partial}{\partial \boldsymbol{\theta}} \mathcal{L}_\dagger(\boldsymbol{\beta}, \boldsymbol{\theta}; \mathbf{y}, \mathbf{X}) &= \frac{1}{2} \text{Tr} \left(\tilde{\boldsymbol{\Sigma}}_\dagger^{-1} \frac{\partial \tilde{\boldsymbol{\Sigma}}_\dagger}{\partial \boldsymbol{\theta}} \right) - \frac{1}{2} (\mathbf{y} - \mathbf{X}\boldsymbol{\beta})^\top \tilde{\boldsymbol{\Sigma}}_\dagger^{-1} \frac{\partial \tilde{\boldsymbol{\Sigma}}_\dagger}{\partial \boldsymbol{\theta}} \tilde{\boldsymbol{\Sigma}}_\dagger^{-1} (\mathbf{y} - \mathbf{X}\boldsymbol{\beta}),\end{aligned}\tag{4}$$

where $\frac{\partial \tilde{\boldsymbol{\Sigma}}_\dagger}{\partial \boldsymbol{\theta}} = \frac{\partial \tilde{\boldsymbol{\Sigma}}_s}{\partial \boldsymbol{\theta}} + \frac{\partial \boldsymbol{\Sigma}_l}{\partial \boldsymbol{\theta}}$ with

$$\begin{aligned}\frac{\partial \tilde{\boldsymbol{\Sigma}}_s}{\partial \boldsymbol{\theta}} &= \left(\frac{\partial \boldsymbol{\Sigma}}{\partial \boldsymbol{\theta}} - \frac{\partial \boldsymbol{\Sigma}_l}{\partial \boldsymbol{\theta}} \right) \circ \mathbf{T}(\gamma) + \frac{\partial \sigma^2}{\partial \boldsymbol{\theta}} \mathbf{I}_n, \\ \frac{\partial \boldsymbol{\Sigma}_l}{\partial \boldsymbol{\theta}} &= \frac{\partial \boldsymbol{\Sigma}_{mn}^\top}{\partial \boldsymbol{\theta}} \boldsymbol{\Sigma}_m^{-1} \boldsymbol{\Sigma}_{mn} + \boldsymbol{\Sigma}_{mn}^\top \boldsymbol{\Sigma}_m^{-1} \frac{\partial \boldsymbol{\Sigma}_{mn}}{\partial \boldsymbol{\theta}} - \boldsymbol{\Sigma}_{mn}^\top \boldsymbol{\Sigma}_m^{-1} \frac{\partial \boldsymbol{\Sigma}_m}{\partial \boldsymbol{\theta}} \boldsymbol{\Sigma}_m^{-1} \boldsymbol{\Sigma}_{mn},\end{aligned}$$

where $\tilde{\boldsymbol{\Sigma}}_s$ denotes the sparse matrix $\boldsymbol{\Sigma}_s + \sigma^2 \mathbf{I}_n$. The evaluation of the negative log-likelihood and its derivatives requires the calculation of linear equations systems and the determinant of the $n \times n$ matrix $\tilde{\boldsymbol{\Sigma}}_\dagger$. Applying the Sherman-Woodbury-Morrison formula, we obtain

$$\tilde{\boldsymbol{\Sigma}}_\dagger^{-1} = (\tilde{\boldsymbol{\Sigma}}_s + \boldsymbol{\Sigma}_{mn}^\top \boldsymbol{\Sigma}_m^{-1} \boldsymbol{\Sigma}_{mn})^{-1} = \tilde{\boldsymbol{\Sigma}}_s^{-1} - \tilde{\boldsymbol{\Sigma}}_s^{-1} \boldsymbol{\Sigma}_{mn}^\top (\boldsymbol{\Sigma}_m + \boldsymbol{\Sigma}_{mn} \tilde{\boldsymbol{\Sigma}}_s^{-1} \boldsymbol{\Sigma}_{mn}^\top)^{-1} \boldsymbol{\Sigma}_{mn} \tilde{\boldsymbol{\Sigma}}_s^{-1}.\tag{5}$$

Moreover, by Sylvester's determinant theorem, the determinant of $\tilde{\boldsymbol{\Sigma}}_\dagger$ can be written as

$$\det(\tilde{\boldsymbol{\Sigma}}_\dagger) = \det(\boldsymbol{\Sigma}_m + \boldsymbol{\Sigma}_{mn} \tilde{\boldsymbol{\Sigma}}_s^{-1} \boldsymbol{\Sigma}_{mn}^\top) \cdot \det(\boldsymbol{\Sigma}_m)^{-1} \cdot \det(\tilde{\boldsymbol{\Sigma}}_s).\tag{6}$$

The computational complexity associated with the computation of the negative log-likelihood and its derivatives is of the order $\mathcal{O}(n \cdot (m^2 + n_\gamma^2) + g(n))$, where we recall that $g(n) \approx n^{3/2}$ for spatial data, see Section 1, and the required storage of order $\mathcal{O}(n \cdot (m + n_\gamma))$, where m represents the number of inducing points and n_γ is the average number of non-zero entries per row in $\tilde{\boldsymbol{\Sigma}}_s$.

2.3 Predictive distribution

The predictive distribution for n_p new locations under the FSA is $\mathcal{N}(\boldsymbol{\mu}_\dagger^p, \boldsymbol{\Sigma}_\dagger^p)$ with

$$\boldsymbol{\mu}_\dagger^p = \mathbf{X}^p \boldsymbol{\beta} + (\boldsymbol{\Sigma}_{nn_p}^\dagger)^\top \tilde{\boldsymbol{\Sigma}}_\dagger^{-1} (\mathbf{y} - \mathbf{X}\boldsymbol{\beta}) \quad \text{and} \quad \boldsymbol{\Sigma}_\dagger^p = \boldsymbol{\Sigma}_{nn_p}^\dagger + \sigma^2 \mathbf{I}_{n_p} - (\boldsymbol{\Sigma}_{nn_p}^\dagger)^\top \tilde{\boldsymbol{\Sigma}}_\dagger^{-1} \boldsymbol{\Sigma}_{nn_p}^\dagger,$$

where $\boldsymbol{\Sigma}_{nn_p}^\dagger = \boldsymbol{\Sigma}_{nn_p}^s + \boldsymbol{\Sigma}_{nn_p}^l$ is the FSA cross-covariance matrix between the prediction locations \mathcal{S}^p and all other observed coordinates \mathcal{S} . The large-scale and short-scale terms are given by

$$\boldsymbol{\Sigma}_{nn_p}^l = \boldsymbol{\Sigma}_{mn}^\top \boldsymbol{\Sigma}_m^{-1} \boldsymbol{\Sigma}_{mn_p} \quad \text{and} \quad \boldsymbol{\Sigma}_{nn_p}^s = (\boldsymbol{\Sigma}_{nn_p} - \boldsymbol{\Sigma}_{nn_p}^l) \circ \mathbf{T}_{nn_p}(\gamma),$$

where $\mathbf{T}_{nn_p}(\gamma) = [c_{\text{taper}}(\|\mathbf{s}_i - \mathbf{s}_j^p\|_2; \gamma)]_{i=1:n, j=1:n_p} \in \mathbb{R}^{n \times n_p}$ and

$\boldsymbol{\Sigma}_{mn_p} = [c(\mathbf{s}_i^*, \mathbf{s}_j^p)]_{i=1:m, j=1:n_p} \in \mathbb{R}^{m \times n_p}$. Moreover, $\boldsymbol{\Sigma}_{n_p}^\dagger = (\boldsymbol{\Sigma}_{n_p} - \boldsymbol{\Sigma}_{mn_p}^\top \boldsymbol{\Sigma}_m^{-1} \boldsymbol{\Sigma}_{mn_p}) \circ$

$\mathbf{T}_{n_p}(\gamma) + \Sigma_{mn_p}^T \Sigma_m^{-1} \Sigma_{mn_p} \in \mathbb{R}^{n_p \times n_p}$ is a covariance matrix with
 $\mathbf{T}_{n_p}(\gamma) = [\text{c}_{\text{taper}} (||\mathbf{s}_i^p - \mathbf{s}_j^p||_2; \gamma)]_{i=1:n_p, j=1:n_p} \in \mathbb{R}^{n_p \times n_p}$.

Assuming that the linear solve $\tilde{\Sigma}_{\dagger}^{-1}(\mathbf{y} - \mathbf{X}\boldsymbol{\beta})$ is precomputed during the parameter estimation, the computational cost for the predictive mean $\boldsymbol{\mu}_{\dagger}^p$ is $\mathcal{O}(n_p \cdot (n_{\gamma}^p + m) + n \cdot m)$, where n_{γ}^p represents the average number of non-zero entries per row in $(\Sigma_{nn_p}^s)^T$. Additionally, assuming that the necessary Cholesky factor is precomputed, the computational complexity of the predictive covariance Σ_{\dagger}^p is $\mathcal{O}(m \cdot n_{\gamma} \cdot n + m \cdot n_{\gamma}^p \cdot n_p + m^2 \cdot n + m^2 \cdot n_p + n \cdot n_p \cdot n_{\gamma} + n \cdot n_p^2)$; see Appendix A for a derivation. Further, the predictive variances

$$\text{diag}(\Sigma_{\dagger}^p) = \sigma_1^2 \mathbf{I}_{n_p} + \sigma^2 \mathbf{I}_{n_p} - \text{diag}((\Sigma_{nn_p}^{\dagger})^T \tilde{\Sigma}_{\dagger}^{-1} \Sigma_{nn_p}^{\dagger}) \in \mathbb{R}^{n_p}, \quad (7)$$

can be calculated in $\mathcal{O}(m \cdot n_{\gamma} \cdot n + m \cdot n_{\gamma}^p \cdot n_p + m^2 \cdot n + m^2 \cdot n_p + n \cdot n_p \cdot n_{\gamma})$ operations; see Appendix A for a derivation. These computations can become prohibitively slow for large n and n_p due to the ‘‘quadratic’’ $n \cdot n_p$ term.

3 Iterative methods for the full-scale approximation

In this section, we show how iterative methods and stochastic approximations can be used for fast inference with the FSA.

3.1 Parameter estimation

To compute linear solves involving $\tilde{\Sigma}_{\dagger}$, we apply the Conjugate Gradient (CG) method. In each iteration of the CG method, we calculate matrix-vector products of the form $(\tilde{\Sigma}_s + \Sigma_{mn}^T \Sigma_m^{-1} \Sigma_{mn})\mathbf{v}$ for $\mathbf{v} \in \mathbb{R}^n$, which require $\mathcal{O}(n \cdot (m + n_{\gamma}))$ operations. To approximate the log-determinant $\log \det(\tilde{\Sigma}_{\dagger})$ in (4), we employ the SLQ method [Ubaru et al., 2017] which combines a quadrature technique based on the Lanczos algorithm with Hutchinson’s estimator [Hutchinson, 1989]:

$$\begin{aligned} \log \det(\tilde{\Sigma}_{\dagger}) &= \text{Tr}(\log(\tilde{\Sigma}_{\dagger})) \approx \frac{1}{\ell} \sum_{i=1}^{\ell} \mathbf{z}_i^T \log(\tilde{\Sigma}_{\dagger}) \mathbf{z}_i \\ &\approx \frac{1}{\ell} \sum_{i=1}^{\ell} \mathbf{z}_i^T \tilde{\mathbf{Q}}_i \log(\tilde{\mathbf{T}}_i) \tilde{\mathbf{Q}}_i^T \mathbf{z}_i = \frac{1}{\ell} \sum_{i=1}^{\ell} \mathbf{e}_1^T \log(\tilde{\mathbf{T}}_i) \mathbf{e}_1, \end{aligned}$$

where $\tilde{\mathbf{Q}}_i \tilde{\mathbf{T}}_i \tilde{\mathbf{Q}}_i^T$ is a partial Lanczos tridiagonalization of $\tilde{\Sigma}_{\dagger}$, where $\tilde{\mathbf{T}}_i \in \mathbb{R}^{k \times k}$ is tridiagonal and $\tilde{\mathbf{Q}}_i \in \mathbb{R}^{n \times k}$ is orthonormal, with initial vector \mathbf{z}_i and rank k , where $\mathbb{E}[\mathbf{z}_i] = \mathbf{0}$ and $\mathbb{E}[\mathbf{z}_i \mathbf{z}_i^T] = \mathbf{I}_n$, for instance, $\mathbf{z}_i \sim \mathcal{N}(\mathbf{0}, \mathbf{I}_n)$. Dong et al. [2017] analyzed different approaches to estimate the log det and found that SLQ is superior to other methods.

As in Gardner et al. [2018], we use the connection between the Lanczos and the CG algorithm to calculate the ℓ partial Lanczos tridiagonal matrices $\tilde{\mathbf{T}}_i$ and thus avoid the necessity for explicitly employing the Lanczos tridiagonalization method. This is advantageous since the Lanczos algorithm can be numerically unstable and can have high storage requirements. In each iteration of this modified CG method, we calculate matrix-matrix products, which involve $\mathcal{O}(n \cdot (m + n_{\gamma}))$ operations.

In addition to the ℓ partial Lanczos tridiagonal matrices, the modified CG method computes the ℓ linear solves $(\tilde{\Sigma}_s + \Sigma_{mn}^T \Sigma_m^{-1} \Sigma_{mn})^{-1} \mathbf{z}_i$ for the probe vectors \mathbf{z}_i . This means that once the log-likelihood is calculated, gradients can be calculated with minimal computational overhead by approximating the trace term in (4) using stochastic trace estimation (STE)

$$\text{Tr} \left(\tilde{\Sigma}_\dagger^{-1} \frac{\partial \tilde{\Sigma}_\dagger}{\partial \boldsymbol{\theta}} \right) \approx \frac{1}{\ell} \sum_{i=1}^{\ell} (\mathbf{z}_i^T \tilde{\Sigma}_\dagger^{-1}) \left(\frac{\partial \tilde{\Sigma}_\dagger}{\partial \boldsymbol{\theta}} \mathbf{z}_i \right).$$

Therefore, we have computational cost for calculating the negative log-likelihood and its derivatives of $\mathcal{O}(n \cdot (m^2 + m \cdot t + n_\gamma \cdot t))$, where t is the used number of iterations in the CG algorithms. The number t has a slight dependence on n , m and n_γ ; see the simulated experiments in Section 4.2 and Theorems 3.2 and 3.3. In Appendix B, we also show how the Fisher information can be calculated efficiently using STE.

3.2 Predictive variances

Calculating predictive variances in (7) is computationally expensive when n and n_p are large, even with iterative methods due to n_p right-hand sides. In Algorithm 1, we propose a more efficient simulation-based approach. This algorithm results in an unbiased and consistent approximation for $\text{diag}(\Sigma_\dagger^p)$, see Appendix A for a proof of Proposition 3.1. The diagonals $\mathbf{D}_1^d, \dots, \mathbf{D}_3^d$ in Algorithm 1 are calculated deterministically using the preconditioned CG method for the linear solves $\Sigma_\dagger^{-1} \Sigma_{mn}^T$ and $\tilde{\Sigma}_s^{-1} \Sigma_{mn}^T$. We estimate the remaining diagonal term $\mathbf{D}_\ell \approx \text{diag}((\Sigma_{nn_p}^s)^T \tilde{\Sigma}_s^{-1} \Sigma_{nn_p}^s)$ stochastically [Bekas et al., 2007], where the linear solves $\tilde{\Sigma}_s^{-1} \Sigma_{nn_p}^s \mathbf{z}_i^{(1)}$ can be done using the preconditioned CG method. The computational complexity of Algorithm 1 is $\mathcal{O}(n_p \cdot (m \cdot n_\gamma^2 + m^2) + n \cdot (m \cdot n_\gamma \cdot t + m^2 \cdot t))$. In addition, the algorithm can be easily parallelized as it relies on matrix-matrix multiplications. Note that we use Rademacher random vectors with entries ± 1 , see Appendix C.

Proposition 3.1. *Algorithm 1 produces an unbiased and consistent estimator \mathbf{D}^p for the predictive variance $\text{diag}(\Sigma_\dagger^p)$ given in (7).*

Algorithm 1 Approximate predictive variances using simulation

Input: Matrices $\Sigma_{nn_p}^s, \Sigma_{mn}, \Sigma_m, \Sigma_{mn_p}, \tilde{\Sigma}_s$

Output: Approximated predictive variances $\mathbf{D}^p \approx \text{diag}(\Sigma_\dagger^p)$

- 1: $\mathbf{D}_1^d \leftarrow \text{diag}(\Sigma_{mn_p}^T \Sigma_m^{-1} \Sigma_{mn} \Sigma_\dagger^{-1} \Sigma_{mn}^T \Sigma_m^{-1} \Sigma_{mn_p})$
 - 2: $\mathbf{D}_2^d \leftarrow \text{diag}((\Sigma_{nn_p}^s)^T \Sigma_\dagger^{-1} \Sigma_{mn}^T \Sigma_m^{-1} \Sigma_{mn_p})$
 - 3: $\mathbf{D}_3^d \leftarrow \text{diag}((\Sigma_{nn_p}^s)^T \tilde{\Sigma}_s^{-1} \Sigma_{mn}^T (\Sigma_m + \Sigma_{mn} \tilde{\Sigma}_s^{-1} \Sigma_{mn}^T)^{-1} (\tilde{\Sigma}_s^{-1} \Sigma_{mn}^T)^T \Sigma_{nn_p}^s)$
 - 4: **for** $i = 1$ to ℓ **do**
 - 5: $\mathbf{z}_i^{(2)} \leftarrow (\Sigma_{nn_p}^s)^T \tilde{\Sigma}_s^{-1} \Sigma_{nn_p}^s \mathbf{z}_i^{(1)}$, where $\mathbf{z}_i^{(1)} \sim \text{Rademacher}$
 - 6: **end for**
 - 7: $\mathbf{D}_\ell \leftarrow \frac{1}{\ell} \sum_{i=1}^{\ell} \mathbf{z}_i^{(1)} \circ \mathbf{z}_i^{(2)} \quad \left(\approx \text{diag}((\Sigma_{nn_p}^s)^T \tilde{\Sigma}_s^{-1} \Sigma_{nn_p}^s) \right)$
 - 8: $\mathbf{D}^p \leftarrow \sigma_1^2 \mathbf{1}_{n_p} + \sigma^2 \mathbf{1}_{n_p} - \mathbf{D}_1^d - 2 \cdot \mathbf{D}_2^d + \mathbf{D}_3^d - \mathbf{D}_\ell$
-

Another approach for approximating the costly diagonal $\text{diag}((\Sigma_{nn_p}^s)^T \tilde{\Sigma}_s^{-1} \Sigma_{nn_p}^s)$ is to use the Lanczos algorithm as proposed by [Pleiss et al. \[2018\]](#):

$$\text{diag}((\Sigma_{nn_p}^s)^T \tilde{\Sigma}_s^{-1} \Sigma_{nn_p}^s) \approx \text{diag}((\Sigma_{nn_p}^s)^T \tilde{\mathbf{Q}}_k^s (\tilde{\mathbf{T}}_k^s)^{-1} (\tilde{\mathbf{Q}}_k^s)^T \Sigma_{nn_p}^s), \quad (8)$$

where $\tilde{\mathbf{Q}}_k^s \in \mathbb{R}^{n \times k}$ and $\tilde{\mathbf{T}}_k^s \in \mathbb{R}^{k \times k}$ denote the partial Lanczos tridiagonalization of $\tilde{\Sigma}_s$. This is currently a state-of-the-art approach in machine learning and allows us to compute the diagonal $\text{diag}((\Sigma_{nn_p}^s)^T \tilde{\Sigma}_s^{-1} \Sigma_{nn_p}^s)$ in $\mathcal{O}(k^2 \cdot (n + n_p) + k \cdot (n_p \cdot n_\gamma^p + n \cdot n_\gamma))$. However, the experiments in this paper show that this approach is considerably less accurate and achieving accurate approximations requires a very high rank k .

3.3 Preconditioner

Iterative methods use preconditioners to improve convergence properties and to reduce variance in stochastic approximations. When using a preconditioner \mathbf{P} , the CG algorithm solves the preconditioned system $\mathbf{P}^{-\frac{1}{2}} \tilde{\Sigma}_\dagger \mathbf{P}^{-\frac{1}{2}} \hat{\mathbf{x}} = \mathbf{P}^{-\frac{1}{2}} \mathbf{b}$ with $\hat{\mathbf{x}} = \mathbf{P}^{\frac{1}{2}} \mathbf{x}$ instead of $\tilde{\Sigma}_\dagger \mathbf{x} = \mathbf{b}$. The corresponding stochastic Lanczos quadrature is given by [\[Gardner et al., 2018\]](#)

$$\log \det(\tilde{\Sigma}_\dagger) = \log \det(\mathbf{P}^{-\frac{1}{2}} \tilde{\Sigma}_\dagger \mathbf{P}^{-\frac{1}{2}}) + \log \det(\mathbf{P}) \approx \frac{1}{\ell} \sum_{i=1}^{\ell} \mathbf{e}_1^T \log(\tilde{\mathbf{T}}_i) \mathbf{e}_1 + \log \det(\mathbf{P}),$$

where $\tilde{\mathbf{T}}_i$ is the partial Lanczos tridiagonal matrix of $\mathbf{P}^{-\frac{1}{2}} \tilde{\Sigma}_\dagger \mathbf{P}^{-\frac{1}{2}}$ with initial vector $\mathbf{z}_i \sim \mathcal{N}(\mathbf{0}, \mathbf{P})$, and the stochastic trace estimation can be computed as follows

$$\begin{aligned} \text{Tr}\left(\tilde{\Sigma}_\dagger^{-1} \frac{\partial \tilde{\Sigma}_\dagger}{\partial \boldsymbol{\theta}}\right) &= \text{Tr}\left(\tilde{\Sigma}_\dagger^{-1} \frac{\partial \tilde{\Sigma}_\dagger}{\partial \boldsymbol{\theta}} \mathbb{E}_{\mathbf{z}_i \sim \mathcal{N}(\mathbf{0}, \mathbf{P})} [\mathbf{P}^{-1} \mathbf{z}_i \mathbf{z}_i^T]\right) \\ &= \mathbb{E}_{\mathbf{z}_i \sim \mathcal{N}(\mathbf{0}, \mathbf{P})} \left[(\mathbf{z}_i^T \tilde{\Sigma}_\dagger^{-1}) \left(\frac{\partial \tilde{\Sigma}_\dagger}{\partial \boldsymbol{\theta}} \mathbf{P}^{-1} \mathbf{z}_i \right) \right] \approx \frac{1}{\ell} \sum_{i=1}^{\ell} (\mathbf{z}_i^T \tilde{\Sigma}_\dagger^{-1}) \left(\frac{\partial \tilde{\Sigma}_\dagger}{\partial \boldsymbol{\theta}} \mathbf{P}^{-1} \mathbf{z}_i \right) = \tilde{T}_\ell. \end{aligned}$$

Further, we can reduce the variance of this stochastic estimate by using the preconditioner \mathbf{P} to build a control variate; see Appendix D. In the FSA, we have a low-rank approximation part $\Sigma_{mn}^T \Sigma_m^{-1} \Sigma_{mn}$ with rank m . We use this to define the fully independent training conditional (FITC) preconditioner as

$$\hat{\mathbf{P}} = \mathbf{D}_s + \Sigma_{mn}^T \Sigma_m^{-1} \Sigma_{mn}, \quad (9)$$

where $\mathbf{D}_s = \text{diag}(\tilde{\Sigma}_s) = \text{diag}(\Sigma - \Sigma_{mn}^T \Sigma_m^{-1} \Sigma_{mn} + \sigma^2 \mathbf{I}_n)$. The latter can also be used as preconditioner $\mathbf{D}_s = \mathbf{P}_s \approx \tilde{\Sigma}_s$ in the computations of the predictive variances as outlined in Section 3.2 where linear solves with $\tilde{\Sigma}_s$ are required. Moreover, \mathbf{P}_s can be used to construct a control variate in the stochastic estimation of the diagonal $\text{diag}((\Sigma_{nn_p}^s)^T \tilde{\Sigma}_s^{-1} \Sigma_{nn_p}^s)$; see Appendix D. Concerning computational costs, $\log \det(\hat{\mathbf{P}})$ and calculating $\text{Tr}\left(\hat{\mathbf{P}}^{-1} \frac{\partial \hat{\mathbf{P}}}{\partial \boldsymbol{\theta}}\right)$ are of complexity $\mathcal{O}(n \cdot m^2)$, while linear solves are of $\mathcal{O}(n \cdot m)$. Moreover, the computational overhead for sampling from $\mathcal{N}(\mathbf{0}, \hat{\mathbf{P}})$ is $\mathcal{O}(n \cdot m)$; see Appendix E.

3.4 Convergence theory

In the following, we analyze the convergence properties of the preconditioned CG method when applied to the FSA. For the following statements and proofs, we denote the Frobenius and the 2-norm (spectral norm) by $\|\cdot\|_F$ and $\|\cdot\|_2$, respectively, and define the vector norm $\|\mathbf{v}\|_{\mathbf{A}} = \sqrt{\mathbf{v}^T \mathbf{A} \mathbf{v}}$ for $\mathbf{v} \in \mathbb{R}^n$ and a positive semi-definite matrix $\mathbf{A} \in \mathbb{R}^{n \times n}$, and we make the following assumptions:

Assumption 1. $n \geq 2$.

Assumption 2. The $m \leq n$ inducing points are sampled uniformly without replacement from the set of locations \mathcal{S} .

Assumption 3. The covariance matrix Σ is of the form $\Sigma_{ij} = \sigma_1^2 \cdot r(\mathbf{s}_i, \mathbf{s}_j)$, where $r(\cdot)$ is positive and continuous, and $r(0) = 1$.

First, we analyze the convergence speed of the CG method for linear solves with $\tilde{\Sigma}_{\dagger}$.

Theorem 3.2. Convergence of the CG method

Let $\tilde{\Sigma}_{\dagger} \in \mathbb{R}^{n \times n}$ be the full-scale approximation of a covariance matrix $\tilde{\Sigma} = \Sigma + \sigma^2 \mathbf{I}_n \in \mathbb{R}^{n \times n}$ with m inducing points and taper range γ , where Σ has eigenvalues $\lambda_1 \geq \dots \geq \lambda_n > 0$. Consider the linear system $\tilde{\Sigma}_{\dagger} \mathbf{u}^* = \mathbf{y}$, where $\mathbf{y} \in \mathbb{R}^n$. Let \mathbf{u}_k be the approximation in the k -th iteration of the CG method. Under Assumptions 1–3, the following holds for the relative error

$$\frac{\|\mathbf{u}^* - \mathbf{u}_k\|_{\tilde{\Sigma}_{\dagger}}}{\|\mathbf{u}^* - \mathbf{u}_0\|_{\tilde{\Sigma}_{\dagger}}} \leq 2 \left(1 + \mathcal{O}_P \left(\sigma \cdot \left((\lambda_{m+1} + \frac{n}{\sqrt{m}} \cdot \sigma_1^2) \cdot \sqrt{n \cdot n_{\gamma}} + \lambda_1 \right)^{-\frac{1}{2}} \right) \right)^{-k},$$

where \mathcal{O}_P is the \mathcal{O} -notation in probability (see Definition F.1 in Appendix F).

For the proof, see Appendix F. Theorem 3.2 shows that selecting a narrower taper range γ leads to improved convergence in the CG method. However, the relationship is more complicated regarding the number of inducing points. While terms such as $\frac{n}{\sqrt{m}}$ and λ_{m+1} decrease with larger m leading to faster convergence, we bound $\|\Sigma_{mn}^T \Sigma_m^{-1} \Sigma_{mn}\|_2$ in the proof of Theorem 3.2 by $\|\Sigma\|_2$ (see Appendix F) and $\|\Sigma_{mn}^T \Sigma_m^{-1} \Sigma_{mn}\|_2$ grows with m . Additionally, we observe that the convergence is slower with decreasing σ^2 and increasing values of λ_1 and λ_{m+1} , which are positively related to the covariance parameters.

Theorem 3.3. Convergence of the CG method with the FITC preconditioner

Let $\tilde{\Sigma}_{\dagger} \in \mathbb{R}^{n \times n}$ be the full-scale approximation of a covariance matrix $\tilde{\Sigma} = \Sigma + \sigma^2 \mathbf{I}_n \in \mathbb{R}^{n \times n}$ with m inducing points and taper range γ , where Σ has eigenvalues $\lambda_1 \geq \dots \geq \lambda_n > 0$. Consider the linear system $\tilde{\Sigma}_{\dagger} \mathbf{u}^* = \mathbf{y}$, where $\mathbf{y} \in \mathbb{R}^n$. Let \mathbf{u}_k be the approximation in the k -th iteration of the preconditioned CG method with the FITC preconditioner. Under Assumptions 1–3, the following holds for the relative error

$$\frac{\|\mathbf{u}^* - \mathbf{u}_k\|_{\tilde{\Sigma}_{\dagger}}}{\|\mathbf{u}^* - \mathbf{u}_0\|_{\tilde{\Sigma}_{\dagger}}} \leq 2 \left(1 + \mathcal{O}_P \left(\sigma^2 \cdot \left((\lambda_{m+1} + \frac{n}{\sqrt{m}} \cdot \sigma_1^2) \cdot \sqrt{n \cdot (n_{\gamma} - 1)} \right)^{-1} \right) \right)^{-k},$$

where \mathcal{O}_P is the \mathcal{O} -notation in probability (see Definition F.1 in Appendix F).

For the proof, see Appendix F. We note that the upper bound for the relative error in Theorem 3.3 also holds for $\frac{\|\mathbf{u}^* - \mathbf{u}_k\|_{\tilde{\Sigma}_s}}{\|\mathbf{u}^* - \mathbf{u}_0\|_{\tilde{\Sigma}_s}}$ using the CG method with preconditioner $\hat{\mathbf{P}}_s = \text{diag}(\tilde{\Sigma}_s)$ to solve the linear system $\tilde{\Sigma}_s \mathbf{u}^* = \mathbf{y}$. Similar to Theorem 3.2, Theorem 3.3 shows that selecting a narrower taper range γ leads to improved convergence in the preconditioned CG method. Notably, this improvement is characterized by a relative error approaching 0 for $\gamma \rightarrow 0$, a logical outcome considering that, in this scenario, $\tilde{\Sigma}_\dagger \xrightarrow{\gamma \rightarrow 0} \hat{\mathbf{P}}$. Furthermore, our findings indicate that the convergence rate of the CG method with the FITC preconditioner does not depend on the largest eigenvalue λ_1 . Consequently, using the FITC preconditioner exhibits less sensitivity to the sample size and the correlation function parametrized, e.g., by a range parameter. Furthermore, a higher number of inducing points m leads even to faster convergence. These theoretical results align with empirical results in our simulation study; see Figure 2.

4 Simulation study

In the following, we analyze our methods in experiments with simulated data. Unless stated otherwise, we simulate $n = 100'000$ samples from a zero-mean GP with a Matérn covariance function with smoothness parameter $\nu = \frac{3}{2}$, marginal variance $\sigma_1^2 = 1$, a nugget effect $\sigma^2 = 1$, and locations samples uniformly on the unit square $[0, 1] \times [0, 1]$. We consider three different choices of effective ranges (0.5, 0.2, 0.05) corresponding to range parameters ρ of approximately $(\frac{0.5}{4.7439}, \frac{0.2}{4.7439}, \frac{0.05}{4.7439}) = (0.1054, 0.0422, 0.0105)$. We use a tolerance level of $\delta = 0.001$ for checking convergence in the CG algorithm, in line with the recommendations of Maddox et al. [2021]. Further, unless specified otherwise, we use $\ell = 50$ sample vectors for the stochastic approximations. All of the following calculations are done with an AMD EPYC 7742 processor and 512 GB of random-access memory using the GPBoost library version 1.3.0 compiled with the GCC compiler version 11.2.0. For reproducibility, the code to reproduce the experiments is available at <https://github.com/TimGyger/iterativeFSA>.

4.1 Methods for choosing inducing points

There are various ways of choosing inducing points. We compare three different methods that do not use any response variable information but only the spatial input locations: random selection, kMeans++ [Arthur and Vassilvitskii, 2007], and the CoverTree algorithm [Terenin et al., 2022]. The computational complexities of these methods are $\mathcal{O}(m)$, $\mathcal{O}(n \cdot m)$, and $\mathcal{O}(n \cdot \log(n))$, respectively. We compare the negative log-likelihood evaluated at the true population parameters over 25 simulation iterations, and all calculations are done using the Cholesky decomposition. In Figure 1, we present the results for the FITC approximation, which combines the predictive process with the diagonal of the residual process for varying numbers of inducing points. We find that the kMeans++ algorithm usually results in the lowest negative log-likelihood for a given number of inducing points. The CoverTree algorithm achieves slightly worse results, and a random selection is clearly inferior. We observe similar results for the FSA; see Figure 7 in Appendix H. Therefore, we use the kMeans++ algorithm in the following to determine the inducing points.

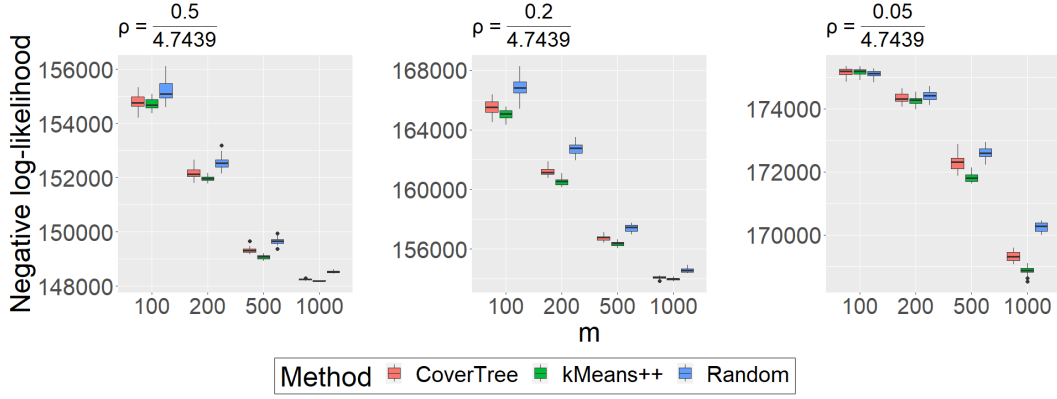


Figure 1: Box-plots of the negative log-likelihood for the FITC approximation for different effective ranges (0.5, 0.2, 0.05 from left to right) and numbers of inducing points m .

4.2 Comparison of preconditioners

Table 1 presents a performance comparison for simulated data using an effective range of 0.2 for the FITC preconditioner and the state-of-the-art general-purpose pivoted Cholesky preconditioner across different ranks $k \in \{200, 500, 1'000\}$. These ranks exceed the recommendations of Maddox et al. [2021]. In Table 5 in Appendix I we present additionally the results for effective ranges of 0.05 and 0.5. We observe that the FITC preconditioner outperforms the pivoted Cholesky preconditioner even for a very high rank k . As a result, we use the FITC preconditioner in the following. In Figure 2, we

Preconditioner:	None	FITC	Pivoted Cholesky		
			$k = 200$	$k = 500$	$k = 1'000$
CG-Iterations	190	14	91	52	32
Time (s)	54	10	52	83	266

Table 1: Number of (preconditioned) CG-iterations for the linear solve $\tilde{\Sigma}_{\dagger}^{-1} \mathbf{y}$ and the time in seconds (s) for computing the negative log-likelihood for the true population parameters.

show the number of iterations required by the CG method with and without the FITC preconditioner for calculating $\tilde{\Sigma}_{\dagger}^{-1} \mathbf{y}$ depending on the parameters n , m , and γ . These results align with Theorems 3.2 and 3.3. In more detail, we observe that the convergence of the CG method with the FITC preconditioner is less sensitive to the sample size than without a preconditioner. Furthermore, the number of iterations in the CG algorithm without a preconditioner increases with a growing number of inducing points m . On the other hand, the number of iterations decreases in m when using the FITC preconditioner. This is consistent with our convergence theorems.

4.3 Comparison of methods for calculating predictive variances

In the following, we compare the approach based on the Lanczos algorithm and our proposed simulation-based approach introduced in Section 3.2 for calculating predictive

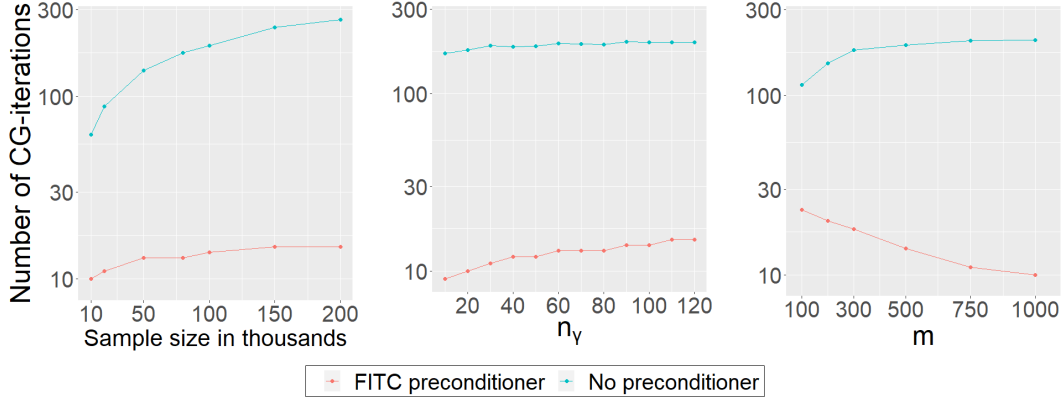


Figure 2: Number of iterations used in the CG method with and without the FITC preconditioner for calculating $\tilde{\Sigma}_\dagger^{-1} \mathbf{y}$ for simulated data with an effective range of 0.2. Left: Different sample sizes n with constant $n_\gamma = 80$ and $m = 500$. Middle: Different taper ranges γ with constant $n = 100'000$ and $m = 500$. Right: Different numbers of inducing points m with constant $n = 100'000$ and $n_\gamma = 80$.

variances. We additionally use data at $n_p = 100'000$ new prediction locations to do this. Evaluation is done using the log-score (LS) $-\log \left(\frac{1}{n_p} \sum_{i=1}^{n_p} \Phi \left(\mathbf{y}_i^*; \boldsymbol{\mu}_{\dagger,i}^p, \sqrt{\boldsymbol{\sigma}_{p,i}^2} \right) \right)$, where $\Phi(x; \mu, \sigma)$ is the cumulative distribution function of a normal distribution with mean μ and variance σ^2 , \mathbf{y}^* is the test response, $\boldsymbol{\mu}_{\dagger}^p$ is the predictive mean, and $\boldsymbol{\sigma}_p^2$ is the predictive variance $\text{diag}(\boldsymbol{\Sigma}_{\dagger}^p)$. We also consider the root-mean-squared-error (RMSE) of the approximate predictive variances compared to the Cholesky-based ones. In Figure 3, we report the results versus time when using varying numbers of ranks k for the Lanczos algorithm and different numbers of samples ℓ for the stochastic approach, with $k, \ell \in \{50, 200, 500, 1'000, 2'000, 5'000\}$. The figure also reports the runtime for calculating the predictive means and variances using the Cholesky factorization. Additionally, we report results for other range parameters and the standard deviations of the stochastic computations in parentheses in Table 3 in Appendix H. The results show that even for a large rank $k = 5'000$, as recommended by Maddox et al. [2021], the Lanczos method is not able to approximate the predictive variance accurately. This limitation arises from the presence of numerous small eigenvalues in the matrix $\tilde{\Sigma}_s$ and, generally, in covariance matrices. On the other hand, the stochastic approach approximates the predictive variance accurately with low variances in its approximations. Therefore, for the following experiments, we use the stochastic approach.

4.4 Accuracy and computational time of parameter estimates and predictive distributions

Next, we analyze the accuracy and speed of parameter estimates and predictive distributions of iterative methods compared to Cholesky-based calculations. Parameter estimates are obtained by minimizing the negative log-likelihood using a limited-memory BFGS (LBFGS) algorithm. We have also tried using Fisher scoring in two variants: one utilizing Cholesky-based computation and the other employing iterative techniques as described in Section 3.1, but both options were slower than the LBFGS algorithm

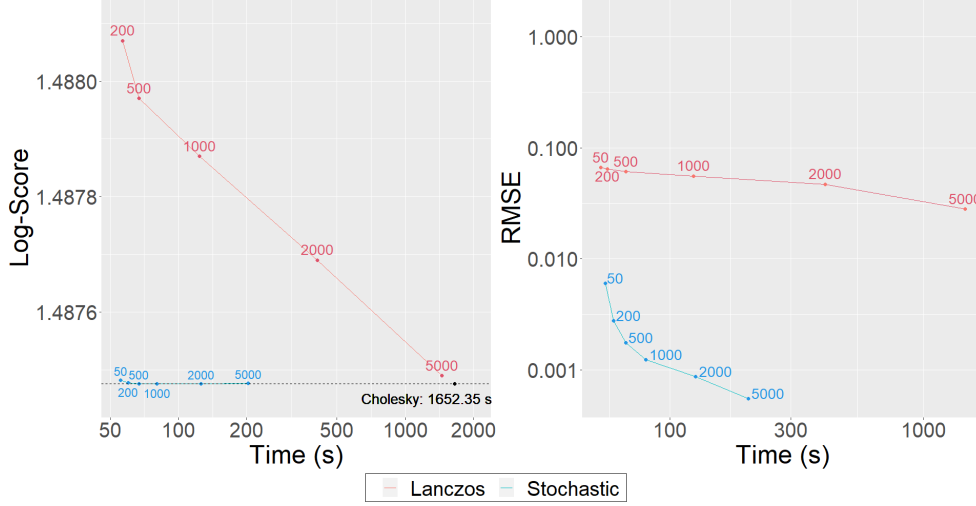


Figure 3: Comparison of the Lanczos and stochastic estimation methods for an effective range of 0.2 and the true population parameters. The dashed black line corresponds to the computations based on Cholesky decomposition. The numbers next to the points correspond to the number of sample vectors or the rank, respectively. For the stochastic approach, the respective mean is shown.

(results not tabulated). For the stochastic estimation of the predictive variance, we use 500 Rademacher sample vectors. For evaluating predictive distributions, we calculate the RMSE, the log-score, and the continuous ranked probability score (CRPS) defined as

$$\frac{1}{n_p} \sum_{i=1}^{n_p} \sigma_{p,i} \left(\frac{1}{\sqrt{\pi}} - 2 \cdot \phi\left(\frac{\mathbf{y}_i^* - \boldsymbol{\mu}_{\dagger,i}^p}{\sigma_{p,i}}; 0, 1\right) - \frac{\mathbf{y}_i^* - \boldsymbol{\mu}_{\dagger,i}^p}{\sigma_{p,i}} \left(2 \cdot \Phi\left(\frac{\mathbf{y}_i^* - \boldsymbol{\mu}_{\dagger,i}^p}{\sigma_{p,i}}; 0, 1\right) - 1 \right) \right),$$

where $\phi(x; \mu, \sigma) = \frac{1}{\sigma\sqrt{2\pi}} \exp\left(-\frac{(x-\mu)^2}{2\sigma^2}\right)$ is the density function of a normal distribution $\mathcal{N}(\mu, \sigma)$. In Figure 4, we present the estimated covariance parameters and the measures for evaluating the predictive distributions over 10 simulated random fields for an effective range of 0.2. We observe virtually identical parameter estimates and prediction accuracy for iterative methods and Cholesky-based computations. Further, iterative methods are faster by approximately one order of magnitude compared to Cholesky-based calculations for both parameter estimation and prediction. Specifically, we find average speed-ups of 7.5, 27.2, and 11.2 for estimating the parameters, computing the predictive distribution, and both together, respectively; see Table 4 in Appendix H. In Table 4 in Appendix H, we also report the bias and RMSE of the estimated covariance parameters for each of the effective ranges 0.5, 0.2, and 0.05, as well as the averages and standard errors of the RMSE of the predictive mean, the log-score, and the CRPS.

In Figure 5, we report runtimes for calculating the negative log-likelihood using both Cholesky-based and iterative methods with the FITC preconditioner ($\ell = 50$) for varying sample sizes, taper ranges, and numbers of inducing points. We observe that the speed-up of the iterative approach grows with the sample size n and the average number of non-zero entries per row n_γ . The speed-up for different numbers of inducing points m is constant. Furthermore, the runtime for the iterative calculations exhibits a linear growth pattern concerning both n and n_γ and a non-linear growth concerning m ,

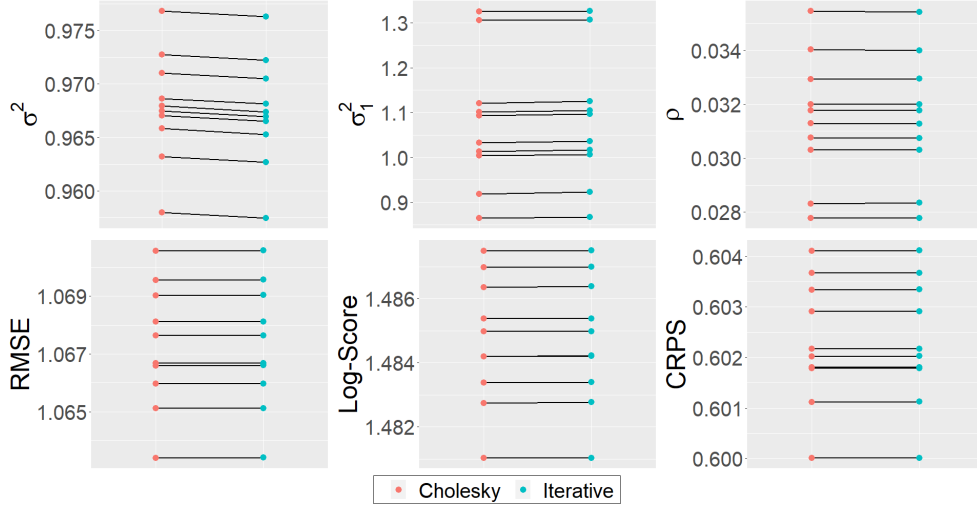


Figure 4: Comparison of the estimated covariance parameters (σ^2 , σ_1^2 , ρ), the RMSE, log-score, and CRPS between the Cholesky-based and the iterative computations.

consistent with the theoretical computational complexity of $\mathcal{O}(n \cdot (m^2 + m \cdot t + n_\gamma \cdot t))$. On the other hand, the runtime for the Cholesky-based calculations is not linear in n , consistent with the theoretical computational complexity of $\mathcal{O}(n \cdot (m^2 + n_\gamma^2) + n^{3/2})$. In Appendix I, we analyze in more detail the accuracy for evaluating the log-likelihood and its derivatives.

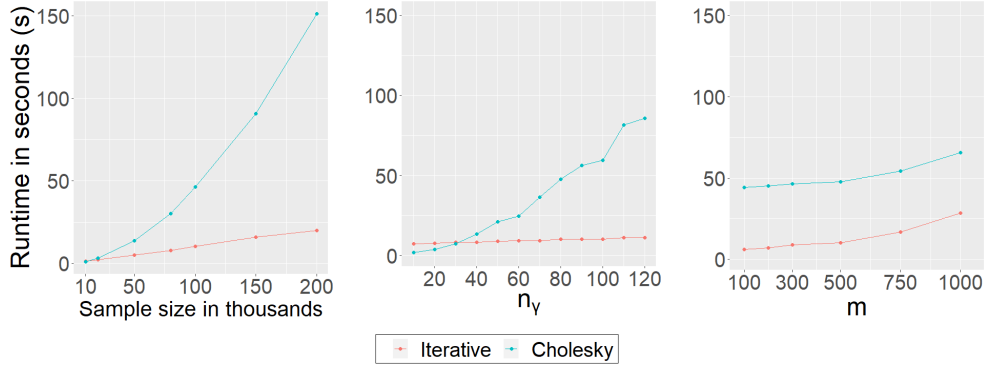


Figure 5: Time (s) for computing the negative log-likelihood by Cholesky-based computations and by the iterative method with the FITC preconditioner for simulated data. Left: Different sample sizes n with constant $n_\gamma = 80$ and $m = 500$. Middle: Different taper ranges γ with constant $n = 100'000$ and $m = 500$. Right: Different numbers of inducing points m with constant $n = 100'000$ and $n_\gamma = 80$.

5 Real-world application

In the following, we apply our proposed methods to real-world data and compare the full-scale approximation to a standalone modified predictive process, or FITC, approximation and covariance tapering. The data set comprises observations of daytime land

surface temperatures in degrees Celsius acquired on August 20, 2023, by the Terra instrument aboard the MODIS satellite (Level-3 data) with a spatial resolution of 1 kilometer (km) on a 1200×1200 km grid, encompassing longitude values from -95.91153 to -91.28381 and latitude values from 34.29519 to 37.06811 . The selection of latitude, longitude ranges, and the date was driven primarily by the minimal cloud cover over the region on that specific date. To generate out-of-sample test data, we designated locations covered by clouds on a different day (September 6, 2023) as test locations. Subsequently, we randomly sample 400'000 data points from the uncovered data set to constitute the training set, while 200'000 data points were randomly selected from the covered data set to form the test set. This sub-sampling enables us to conduct Cholesky-based computations within a reasonable time. Figure 14 in Appendix J shows the full and the sub-sampled training data sets. Figure 15 reports the test data. For the sake of reproducibility, both the data and the downloading code are available on GitHub at <https://github.com/TimGyger/iterativeFSA>. We use $m = 500$ inducing points determined by the kMeans++ algorithm for both the full-scale and FITC approximations, and we set the taper range to $\gamma = 7500$, resulting in an average of $n_\gamma = 80$ non-zero entries per row for both the full-scale and covariance tapering approximations. The mean function is assumed to be linear in the coordinates, $F(\mathbf{X}) = \mathbf{X}\boldsymbol{\beta}$, and we use the coordinates as covariates. In our iterative approach with the FITC preconditioner, we use a convergence tolerance level $\delta = 1$ in the CG algorithm, and we use $\ell = 50$ Gaussian sample vectors for the stochastic estimates. Using lower convergence tolerance levels and less random vectors gives virtually identical results (see below). Furthermore, for the stochastic estimation of the predictive variance, we utilize 500 Rademacher sample vectors. For parameter estimation, we use the same optimization method and settings as in Subsection 4.4. In Table 2, we report the prediction accuracy measures and computation times; see Table 6 in Appendix J for the estimated parameters. We find that the iterative methods result in almost identical parameter estimates and prediction accuracy measures while being approximately one order of magnitude faster than Cholesky-based computations. As expected, the FITC and covariance tapering approximations are faster than the full-scale approximation for the Cholesky-based computations. However, these approximations have considerably worse prediction accuracy than the full-scale approximation. This is most likely due to the inability of these two approximations to capture both the short-scale and large-scale dependencies present in the data. Figures 15 and 16 in Appendix J illustrate the predictive means and variances of different covariance matrix approximation approaches and methodologies. These maps visually confirm the results from Table 2. We see that the FITC approximation's predictive mean is smooth and captures the large-scale spatial structure, but misses the rough short-scale dependence. The tapering approximation is unable to make good predictions at locations where there is no observed data nearby. In such cases, the fixed effects contribute almost exclusively to the prediction. In particular, FSA predicts the spatial structure more accurately than tapering and the FITC approximation. Additionally, Table 7 in Appendix H presents the results for various convergence tolerance levels and sample vectors. We find that, even when employing a higher convergence tolerance and fewer sample vectors, we lose almost no accuracy in parameter estimates and predictive distributions with an increased speed-up.

		FSA		Tapering	FITC
		Iterative	Cholesky	Cholesky	Cholesky
Estimation	Time (s)	5054	33212	13086	12445
	Speed-up	6.6		2.5	2.7
Prediction	RMSE	1.4177	1.4175	2.3349	1.8171
	Log-Score	1.7244	1.7245	2.1735	1.9444
	CRPS	0.75451	0.75449	1.2723	0.94036
	Time (s)	587	5513	199	67.55
	Speed-up	9.4		27.8	81.6
Total	Time (s)	5641	38725	13285	12512
	Speed-up	6.9		2.9	3.1

Table 2: Real-world satellite data results.

6 Conclusion

We propose to use iterative methods for doing inference with a full-scale approximation. In particular, we introduce a novel and efficient preconditioner, called FITC preconditioner, which leverages the structure of the full-scale approximation. In our theoretical analysis, we demonstrate that the application of the proposed preconditioner considerably mitigates the sensitivity of the CG method’s convergence rate with respect to the full-scale approximation parameters (number of inducing points m and taper range γ) as well as the eigenvalue structure of the original covariance matrix. In a comprehensive simulation study, we demonstrate the superior efficiency of the FITC preconditioner compared to the state-of-the-art pivoted Cholesky preconditioner. Additionally, we highlight its utility as a control variate reducing variance in stochastic gradient approximations. Furthermore, we introduce a novel simulation-based method for calculating predictive variances and illustrate its superiority in accuracy and speed over the state-of-the-art Lanczos method. In both simulated and real-world data experiments, we find that our proposed methodology achieves the same level of accuracy as Cholesky-based computations with a substantial reduction in computational time of approximately one order of magnitude.

Appendices

A Predictive (co-)variances within full-scale approximation

The predictive covariance matrix is given by

$$\begin{aligned}
\Sigma_{\dagger}^p &= \Sigma_{n_p}^{\dagger} + \sigma^2 \mathbf{I}_{n_p} - (\Sigma_{nn_p}^{\dagger})^T \tilde{\Sigma}_{\dagger}^{-1} \Sigma_{nn_p}^{\dagger} \\
&= \Sigma_{n_p}^{\dagger} + \sigma^2 \mathbf{I}_{n_p} - (\Sigma_{nn_p}^s)^T \tilde{\Sigma}_s^{-1} \Sigma_{nn_p}^s \\
&\quad - (\Sigma_{mn}^T \Sigma_m^{-1} \Sigma_{mn_p})^T \tilde{\Sigma}_s^{-1} \Sigma_{mn}^T \Sigma_m^{-1} \Sigma_{mn_p} \\
&\quad - (\Sigma_{nn_p}^s)^T \tilde{\Sigma}_s^{-1} \Sigma_{mn}^T \Sigma_m^{-1} \Sigma_{mn_p} \\
&\quad - ((\Sigma_{nn_p}^s)^T \tilde{\Sigma}_s^{-1} \Sigma_{mn}^T \Sigma_m^{-1} \Sigma_{mn_p})^T \\
&\quad + (\Sigma_{nn_p}^s)^T \tilde{\Sigma}_s^{-1} \Sigma_{mn}^T \mathbf{M}^{-1} \Sigma_{mn} \tilde{\Sigma}_s^{-1} \Sigma_{nn_p}^s \\
&\quad + (\Sigma_{mn}^T \Sigma_m^{-1} \Sigma_{mn_p})^T \tilde{\Sigma}_s^{-1} \Sigma_{mn}^T \mathbf{M}^{-1} \Sigma_{mn} \tilde{\Sigma}_s^{-1} \Sigma_{mn}^T \Sigma_m^{-1} \Sigma_{mn_p} \\
&\quad + (\Sigma_{nn_p}^s)^T \tilde{\Sigma}_s^{-1} \Sigma_{mn}^T \mathbf{M}^{-1} \Sigma_{mn} \tilde{\Sigma}_s^{-1} \Sigma_{mn}^T \Sigma_m^{-1} \Sigma_{mn_p} \\
&\quad + ((\Sigma_{nn_p}^s)^T \tilde{\Sigma}_s^{-1} \Sigma_{mn}^T \mathbf{M}^{-1} \Sigma_{mn} \tilde{\Sigma}_s^{-1} \Sigma_{mn}^T \Sigma_m^{-1} \Sigma_{mn_p})^T.
\end{aligned}$$

Presuming the Cholesky factors of $\tilde{\Sigma}_s$ and $\mathbf{M} = (\Sigma_m + \Sigma_{mn} \tilde{\Sigma}_s^{-1} \Sigma_{mn}^T)$ are precomputed during training, the costs for computing the single terms are

1. $(\Sigma_{nn_p}^s)^T \tilde{\Sigma}_s^{-1} \Sigma_{nn_p}^s$: $\mathcal{O}(n \cdot n_p \cdot n_{\gamma} + n \cdot n_p^2)$,
2. $(\Sigma_{mn}^T \Sigma_m^{-1} \Sigma_{mn_p})^T \tilde{\Sigma}_s^{-1} \Sigma_{mn}^T \Sigma_m^{-1} \Sigma_{mn_p}$: $\mathcal{O}(m \cdot n_{\gamma} \cdot n + m^2 \cdot n + m^2 \cdot n_p + m \cdot n_p^2)$,
3. $(\Sigma_{nn_p}^s)^T \tilde{\Sigma}_s^{-1} \Sigma_{mn}^T \Sigma_m^{-1} \Sigma_{mn_p}$: $\mathcal{O}(m \cdot n_{\gamma} \cdot n + m^2 \cdot n_p + m \cdot n_{\gamma}^p \cdot n_p + m \cdot n_p^2)$,
4. $(\Sigma_{nn_p}^s)^T \tilde{\Sigma}_s^{-1} \Sigma_{mn}^T \mathbf{M}^{-1} \Sigma_{mn} \tilde{\Sigma}_s^{-1} \Sigma_{nn_p}^s$:
 $\mathcal{O}(m \cdot n_{\gamma} \cdot n + m^2 \cdot n + m \cdot n_{\gamma}^p \cdot n_p + m \cdot n_p^2)$,
5. $(\Sigma_{mn}^T \Sigma_m^{-1} \Sigma_{mn_p})^T \tilde{\Sigma}_s^{-1} \Sigma_{mn}^T \mathbf{M}^{-1} \Sigma_{mn} \tilde{\Sigma}_s^{-1} \Sigma_{mn}^T \Sigma_m^{-1} \Sigma_{mn_p}$:
 $\mathcal{O}(m \cdot n_{\gamma} \cdot n + m^2 \cdot n + m^2 \cdot n_p + m \cdot n_p^2)$,
6. $(\Sigma_{nn_p}^s)^T \tilde{\Sigma}_s^{-1} \Sigma_{mn}^T \mathbf{M}^{-1} \Sigma_{mn} \tilde{\Sigma}_s^{-1} \Sigma_{mn}^T \Sigma_m^{-1} \Sigma_{mn_p}$:
 $\mathcal{O}(m \cdot n_{\gamma} \cdot n + m \cdot n_{\gamma}^p \cdot n_p + m^2 \cdot n + m^2 \cdot n_p + m \cdot n_p^2)$.

Therefore, the computational complexity for computing the predictive covariance is

$$\mathcal{O}(m \cdot n_{\gamma} \cdot n + m \cdot n_{\gamma}^p \cdot n_p + m^2 \cdot n + m^2 \cdot n_p + n \cdot n_p \cdot n_{\gamma} + n \cdot n_p^2),$$

and for the predictive variances is

$$\mathcal{O}(m \cdot n_{\gamma} \cdot n + m \cdot n_{\gamma}^p \cdot n_p + m^2 \cdot n + m^2 \cdot n_p + n \cdot n_p \cdot n_{\gamma}).$$

For the case when $n_p > n$, we obtain

$$\mathcal{O}(n_p \cdot (m \cdot n_{\gamma}^p + m^2 + n \cdot n_p)) \quad \text{and} \quad \mathcal{O}(n_p \cdot (m \cdot n_{\gamma}^p + m^2 + n \cdot n_{\gamma})),$$

respectively. And for the case when $n_p < n$, we obtain

$$\mathcal{O}(n \cdot (m \cdot n_\gamma + m^2 + n_p \cdot n_\gamma + n_p^2)) \quad \text{and} \quad \mathcal{O}(n \cdot (m \cdot n_\gamma + m^2 + n_p \cdot n_\gamma)),$$

respectively.

B Fisher scoring

The Fisher information matrix $\mathbf{I} \in \mathbb{R}^{q \times q}$ for Fisher scoring is given by

$$(\mathbf{I})_{kl} = \frac{1}{2} \text{Tr} \left(\tilde{\Sigma}_\dagger^{-1} \frac{\partial \tilde{\Sigma}_\dagger}{\partial \theta_k} \tilde{\Sigma}_\dagger^{-1} \frac{\partial \tilde{\Sigma}_\dagger}{\partial \theta_l} \right), \quad 1 \leq k, l \leq q.$$

These trace terms can be computed by using STE

$$\text{Tr} \left(\tilde{\Sigma}_\dagger^{-1} \frac{\partial \tilde{\Sigma}_\dagger}{\partial \theta_k} \tilde{\Sigma}_\dagger^{-1} \frac{\partial \tilde{\Sigma}_\dagger}{\partial \theta_l} \right) \approx \frac{1}{\ell} \sum_{i=1}^{\ell} (\mathbf{z}_i^\top \tilde{\Sigma}_\dagger^{-1} \frac{\partial \tilde{\Sigma}_\dagger}{\partial \theta_k}) (\tilde{\Sigma}_\dagger^{-1} \frac{\partial \tilde{\Sigma}_\dagger}{\partial \theta_l} \mathbf{z}_i), \quad 1 \leq k, l \leq q,$$

where the linear solves $\tilde{\Sigma}_\dagger^{-1} \mathbf{z}_i$ and $\tilde{\Sigma}_\dagger^{-1} \frac{\partial \tilde{\Sigma}_\dagger}{\partial \theta_l} \mathbf{z}_i$ can be computed by the CG method or in the Cholesky-based variant using the Sherman-Woodbury-Morrison formula and the Cholesky factor of $\tilde{\Sigma}_s$.

C Approximate predictive variances using simulation

Note that we use Rademacher random vectors with entries ± 1 since the stochastic approximation of the diagonal of a matrix $\mathbf{A} \in \mathbb{R}^{n \times n}$ with Gaussian random vectors \mathbf{z}_i is given by

$$\text{diag}(\mathbf{A}) \approx \left[\sum_{i=1}^{\ell} \mathbf{z}_i \circ \mathbf{A} \mathbf{z}_i \right] \oslash \left[\sum_{i=1}^{\ell} \mathbf{z}_i \circ \mathbf{z}_i \right],$$

where the operator \oslash refers to the elementwise division (Hadamard division).

Therefore, the normalization of a single sample $\mathbf{z}_i \circ \mathbf{A} \mathbf{z}_i$ by all sample vectors \mathbf{z}_i renders it impractical to compute the optimal scaling factor $\hat{\mathbf{c}}_{\text{opt}}$ for applying variance reduction as introduced in the following subsection.

Proof of Proposition 3.1. By standard results, the only non-deterministic term $\frac{1}{\ell} \sum_{i=1}^{\ell} \mathbf{z}_i^{(1)} \circ (\Sigma_{nn_p}^s)^\top \tilde{\Sigma}_s^{-1} \Sigma_{nn_p}^s \mathbf{z}_i^{(1)}$ in Algorithm 1 is an unbiased and consistent estimator for $\text{diag}((\Sigma_{nn_p}^s)^\top \tilde{\Sigma}_s^{-1} \Sigma_{nn_p}^s)$, and the claim in Proposition 3.1 thus follows. \square

D Preconditioner as control variate

$$\begin{aligned} \text{Tr} \left(\tilde{\Sigma}_\dagger^{-1} \frac{\partial \tilde{\Sigma}_\dagger}{\partial \theta} \right) &\approx \frac{1}{\ell} \sum_{i=1}^{\ell} \left((\mathbf{z}_i^\top \tilde{\Sigma}_\dagger^{-1}) \left(\frac{\partial \tilde{\Sigma}_\dagger}{\partial \theta} \mathbf{P}^{-1} \mathbf{z}_i \right) - \hat{\mathbf{c}}_{\text{opt}} \cdot (\mathbf{z}_i^\top \mathbf{P}^{-1}) \left(\frac{\partial \mathbf{P}}{\partial \theta} \mathbf{P}^{-1} \mathbf{z}_i \right) \right) \\ &\quad + \hat{\mathbf{c}}_{\text{opt}} \cdot \text{Tr} \left(\mathbf{P}^{-1} \frac{\partial \mathbf{P}}{\partial \theta} \right), \end{aligned} \tag{10}$$

where

$$\hat{c}_{opt} = \frac{\sum_{i=1}^{\ell} \left((z_i^T \tilde{\Sigma}_{\dagger}^{-1}) \left(\frac{\partial \tilde{\Sigma}_{\dagger}}{\partial \theta} P^{-1} z_i \right) - \tilde{T}_{\ell} \right) (z_i^T P^{-1}) \left(\frac{\partial P}{\partial \theta} P^{-1} z_i \right)}{\sum_{i=1}^{\ell} \left((z_i^T P^{-1}) \left(\frac{\partial P}{\partial \theta} P^{-1} z_i \right) \right)^2}.$$

$$\begin{aligned} \text{diag}((\Sigma_{nn_p}^s)^T \tilde{\Sigma}_s^{-1} \Sigma_{nn_p}^s) &\approx \frac{1}{\ell} \sum_{i=1}^{\ell} \left(z_i \circ ((\Sigma_{nn_p}^s)^T \tilde{\Sigma}_s^{-1} \Sigma_{nn_p}^s z_i) \right. \\ &\quad \left. - \hat{c}_{opt} \circ z_i \circ ((\Sigma_{nn_p}^s)^T P_s^{-1} \Sigma_{nn_p}^s z_i) \right) \\ &\quad + \hat{c}_{opt} \circ \text{diag}((\Sigma_{nn_p}^s)^T P_s^{-1} \Sigma_{nn_p}^s), \end{aligned}$$

where

$$\begin{aligned} \hat{c}_{opt} &= \left(\sum_{i=1}^{\ell} \left(z_i \circ (\Sigma_{nn_p}^s)^T \tilde{\Sigma}_s^{-1} \Sigma_{nn_p}^s z_i - D_{\ell} \right) (z_i \circ (\Sigma_{nn_p}^s)^T P_s^{-1} \Sigma_{nn_p}^s z_i) \right) \\ &\quad \oslash \left(\sum_{i=1}^{\ell} (z_i \circ (\Sigma_{nn_p}^s)^T P_s^{-1} \Sigma_{nn_p}^s z_i)^2 \right). \end{aligned}$$

E Runtime of the FITC preconditioner

Time complexity of computing $\log \det(\hat{P})$, $\text{Tr}(\hat{P}^{-1} \frac{\partial \hat{P}}{\partial \theta})$ and $\hat{P}^{-1} \mathbf{y}$:

To compute the log determinant of the preconditioner, we make use of Sylvester's determinant theorem [Sylvester, 1851]

$$\begin{aligned} \det(\hat{P}) &= \det(D_s + \Sigma_{mn}^T \Sigma_m^{-1} \Sigma_{mn}) \\ &= \det(\Sigma_m + \Sigma_{mn} D_s^{-1} \Sigma_{mn}^T) \cdot \det(\Sigma_m)^{-1} \cdot \det(D_s). \end{aligned}$$

After calculating $\Sigma_m + \Sigma_{mn} D_s^{-1} \Sigma_{mn}^T \in \mathbb{R}^{m \times m}$ in $\mathcal{O}(n \cdot m^2)$, we obtain its Cholesky factor in $\mathcal{O}(m^3)$. As a result, the computation of $\log \det(\hat{P})$ requires $\mathcal{O}(n \cdot m^2)$ time.

For computing the trace $\text{Tr}(\hat{P}^{-1} \frac{\partial \hat{P}}{\partial \theta})$, we can proceed similar.

To compute linear solves with the preconditioner, we make use of the Sherman-Woodbury-Morrison formula [Woodbury, 1950]

$$\begin{aligned} \hat{P}^{-1} \mathbf{y} &= (D_s + \Sigma_{mn}^T \Sigma_m^{-1} \Sigma_{mn})^{-1} \mathbf{y} \\ &= D_s^{-1} \mathbf{y} - D_s^{-1} \Sigma_{mn}^T (\Sigma_m + \Sigma_{mn} D_s^{-1} \Sigma_{mn}^T)^{-1} \Sigma_{mn} D_s^{-1} \mathbf{y}. \end{aligned}$$

After computing $D_s^{-1} \mathbf{y}$ in linear time $\mathcal{O}(n)$, the operation $\Sigma_{mn} D_s^{-1} \mathbf{y}$ necessitates a time complexity of $\mathcal{O}(n \cdot m)$. Subsequently, when we use $\Sigma_m + \Sigma_{mn} D_s^{-1} \Sigma_{mn}^T \in \mathbb{R}^{m \times m}$ and its Cholesky factor computed already for the log determinant, performing a linear solve using this factor requires $\mathcal{O}(m^2)$ time. As a result, following these precomputations, each solving operation with the preconditioner \hat{P} incurs a total time complexity of $\mathcal{O}(n \cdot m)$.

Time complexity of drawing samples from $\mathcal{N}(\mathbf{0}, \hat{\mathbf{P}})$:

We draw samples from $\mathcal{N}(\mathbf{0}, \hat{\mathbf{P}})$ via the reparameterization trick used by [Gardner et al. \[2018\]](#) in Appendix C.1. If $\epsilon_1 \in \mathbb{R}^m$ and $\epsilon_2 \in \mathbb{R}^n$ are standard normal vectors, then $(\Sigma_{mn}^T \Sigma_m^{-\frac{1}{2}} \epsilon_1 + \mathbf{D}_s^{\frac{1}{2}} \epsilon_2)$, is a sample from $\mathcal{N}(\mathbf{0}, \mathbf{D}_s + \Sigma_{mn}^T \Sigma_m^{-1} \Sigma_{mn})$, where $\Sigma_m^{\frac{1}{2}}$ is the Cholesky factor of Σ_m and $\mathbf{D}_s^{\frac{1}{2}}$ is the elementwise square-root of \mathbf{D}_s . Assuming the Cholesky factor is already computed, sampling from $\mathcal{N}(\mathbf{0}, \hat{\mathbf{P}})$ requires matrix-vector multiplications for a total of $\mathcal{O}(n \cdot m)$ time.

F Convergence analysis of the CG method with and without the FITC preconditioner

Definition F.1. Big \mathcal{O} in probability notation

For a set of random variables X_i and a corresponding set of constants a_i both indexed by i , the notation

$$X_i = \mathcal{O}_P(a_i)$$

means that the set of values X_i/a_i is stochastically bounded. That is, for any $\varepsilon > 0$, there exists a finite $M > 0$ and a finite $N > 0$ such that

$$\mathbb{P}\left(\left|\frac{X_i}{a_i}\right| > M\right) < \varepsilon, \forall i \geq N.$$

Lemma F.1. Error bound for Nyström low-rank approximation

Under Assumptions 1–3, let $\Sigma_{mn}^T \Sigma_m^{-1} \Sigma_{mn}$ be the rank- m approximation of a covariance matrix Σ with eigenvalues $\lambda_1 \geq \dots \geq \lambda_n > 0$ as described in Section 2.1. Then, the following inequality holds

$$\|\Sigma - \Sigma_{mn}^T \Sigma_m^{-1} \Sigma_{mn}\|_2 \leq \mathcal{O}_P\left(\lambda_{m+1} + \frac{n}{\sqrt{m}} \cdot \sigma_1^2\right),$$

where \mathcal{O}_P is the \mathcal{O} -notation in probability.

Proof. We start using Theorem 2 in [Kumar et al. \[2012\]](#), which states that with probability at least $1 - \epsilon$, the following inequality holds for any m

$$\begin{aligned} \|\Sigma - \Sigma_{mn}^T \Sigma_m^{-1} \Sigma_{mn}\|_2 &\leq \|\Sigma - \hat{\Sigma}_m\|_2 \\ &+ \frac{2 \cdot n}{\sqrt{m}} \max_i(\Sigma_{ii}) \left(1 + \sqrt{\frac{n-m}{n-\frac{1}{2}} \frac{\log(\frac{1}{\epsilon})}{\beta(m, n)} \frac{d_{\max}^{\Sigma}}{\max_i(L_{ii})}}\right), \end{aligned}$$

where $\hat{\Sigma}_m$ is the best rank- m approximation of Σ with respect to the spectral norm $\|\cdot\|_2$, $\beta(m, n) = 1 - \frac{1}{2 \cdot \max(m, n-m)}$, L_{ii} is the i -th entry of the diagonal of the Cholesky factor \mathbf{L} of Σ and $d_{\max}^{\Sigma} = \max_{ij} \sqrt{\Sigma_{ii} + \Sigma_{jj} - 2 \cdot \Sigma_{ij}}$.

By the Eckart-Young-Mirsky theorem for the spectral norm [[Eckart and Young, 1936](#)], we know that the best rank- m approximation of Σ in the spectral norm is

its m -truncated eigenvalue decomposition considering only the m largest eigenvalues. Therefore, we obtain

$$\|\Sigma - \hat{\Sigma}_m\|_2 \leq \lambda_{m+1},$$

where λ_{m+1} is the $(m+1)$ -th largest eigenvalue of Σ .

Since $\Sigma_{ij} \geq 0$ for all $i, j = 1, \dots, n$ and Σ has by Assumption 3 a constant diagonal with entries equal to σ_1^2 , we have $d_{\max}^{\Sigma} \leq \sqrt{2 \cdot \Sigma_{ii}} = \sqrt{2} \cdot \sqrt{\sigma_1^2}$. Moreover, by the Cholesky decomposition algorithm, we have $\max_i(L_{ii}) = \sqrt{\sigma_1^2}$. Hence, we obtain

$$\begin{aligned} \|\Sigma - \Sigma_{mn}^T \Sigma_m^{-1} \Sigma_{mn}\|_2 &\leq \lambda_{m+1} + \frac{2 \cdot n}{\sqrt{m}} \cdot \sigma_1^2 \cdot \left(1 + \sqrt{\frac{n-m}{n-\frac{1}{2}} \frac{\log(\frac{1}{\epsilon})}{\beta(m, n)}} \frac{\sqrt{2} \cdot \sqrt{\sigma_1^2}}{\sqrt{\sigma_1^2}}\right) \\ &= \lambda_{m+1} + \frac{2 \cdot n}{\sqrt{m}} \cdot \sigma_1^2 \cdot \left(1 + \sqrt{2 \cdot \frac{n-m}{n-\frac{1}{2}} \frac{\log(\frac{1}{\epsilon})}{\beta(m, n)}}\right). \end{aligned}$$

Since $\max(m, n-m) \geq \frac{n}{2}$, we have $\frac{1}{\beta(m, n)} = \frac{1}{1 - \frac{1}{2 \cdot \max(m, n-m)}} \leq \frac{1}{1 - \frac{1}{n}} = \frac{n}{n-1} \leq 2$. Hence, we obtain

$$\begin{aligned} \|\Sigma - \Sigma_{mn}^T \Sigma_m^{-1} \Sigma_{mn}\|_2 &\leq \lambda_{m+1} + \frac{2 \cdot n}{\sqrt{m}} \cdot \sigma_1^2 \cdot \left(1 + \sqrt{4 \cdot \frac{n-m}{n-\frac{1}{2}} \log\left(\frac{1}{\epsilon}\right)}\right) \\ &\leq \lambda_{m+1} + \frac{2 \cdot n}{\sqrt{m}} \cdot \sigma_1^2 \cdot \left(1 + \sqrt{\frac{8}{3} \cdot (n-m) \cdot \log\left(\frac{1}{\epsilon}\right)}\right). \end{aligned}$$

To use the \mathcal{O} -notation in probability in Definition F.1, we have to show that there exists an N such that for all $m \geq N$ it holds that $(n-m) \cdot \log\left(\frac{1}{\epsilon}\right)$ is finite.

We obtain for a constant $C > 0$

$$(n-m) \cdot \log\left(\frac{1}{\epsilon}\right) \leq C \iff m \geq n - \frac{C}{\log\left(\frac{1}{\epsilon}\right)},$$

and therefore, $N = \max\left(n - \frac{C}{\log\left(\frac{1}{\epsilon}\right)}, 1\right)$.

Using the following equivalence

$$\begin{aligned} \mathbb{P}\left(\left|\frac{\|\Sigma - \Sigma_{mn}^T \Sigma_m^{-1} \Sigma_{mn}\|_2}{\lambda_{m+1} + \frac{2 \cdot n}{\sqrt{m}} \cdot \sigma_1^2 \cdot \left(1 + \sqrt{\frac{8}{3} \cdot (n-m) \cdot \log\left(\frac{1}{\epsilon}\right)}\right)}\right| \leq 1\right) &> 1 - \epsilon \\ \iff \\ \mathbb{P}\left(\left|\frac{\|\Sigma - \Sigma_{mn}^T \Sigma_m^{-1} \Sigma_{mn}\|_2}{\lambda_{m+1} + \frac{2 \cdot n}{\sqrt{m}} \cdot \sigma_1^2 \cdot \left(1 + \sqrt{\frac{8}{3} \cdot (n-m) \cdot \log\left(\frac{1}{\epsilon}\right)}\right)}\right| > 1\right) &< \epsilon, \end{aligned}$$

we have for all $m \geq \max\left(n - \frac{C}{\log\left(\frac{1}{\epsilon}\right)}, 1\right)$ that

$$\begin{aligned} \epsilon &> \mathbb{P}\left(\left|\frac{\|\Sigma - \Sigma_{mn}^T \Sigma_m^{-1} \Sigma_{mn}\|_2}{\lambda_{m+1} + \frac{2 \cdot n}{\sqrt{m}} \cdot \sigma_1^2 \cdot \left(1 + \sqrt{\frac{8}{3}} \cdot (n - m) \cdot \log\left(\frac{1}{\epsilon}\right)\right)}\right| > 1\right) \\ &\geq \mathbb{P}\left(\left|\frac{\|\Sigma - \Sigma_{mn}^T \Sigma_m^{-1} \Sigma_{mn}\|_2}{\lambda_{m+1} + \frac{2 \cdot n}{\sqrt{m}} \cdot \sigma_1^2 \cdot \left(1 + \sqrt{\frac{8}{3}} \cdot C\right)}\right| > 1\right) \\ &\geq \mathbb{P}\left(\left|\frac{\|\Sigma - \Sigma_{mn}^T \Sigma_m^{-1} \Sigma_{mn}\|_2}{\lambda_{m+1} + \frac{n}{\sqrt{m}} \cdot \sigma_1^2}\right| > M\right), \end{aligned}$$

with $M = 2 \cdot \left(1 + \sqrt{\frac{8}{3}} \cdot C\right)$. Hence, we obtain

$$\|\Sigma - \Sigma_{mn}^T \Sigma_m^{-1} \Sigma_{mn}\|_2 = \mathcal{O}_P\left(\lambda_{m+1} + \frac{n}{\sqrt{m}} \cdot \sigma_1^2\right).$$

□

Lemma F.2. Bound for the Condition Number of $\tilde{\Sigma}_\dagger$

Let $\tilde{\Sigma}_\dagger \in \mathbb{R}^{n \times n}$ be the FSA of a covariance matrix $\tilde{\Sigma} = \Sigma + \sigma^2 I_n \in \mathbb{R}^{n \times n}$ with m inducing points and taper range γ , where Σ has eigenvalues $\lambda_1 \geq \dots \geq \lambda_n > 0$. Under Assumptions 1–3, the condition number $\kappa(\tilde{\Sigma}_\dagger)$ is bounded by

$$\kappa(\tilde{\Sigma}_\dagger) \leq \mathcal{O}_P\left(\frac{1}{\sigma^2} \cdot \left((\lambda_{m+1} + \frac{n}{\sqrt{m}} \cdot \sigma_1^2) \cdot \sqrt{n \cdot n_\gamma} + \lambda_1\right)\right) + 1,$$

where n_γ is the average number of non-zero entries per row in $\mathbf{T}(\gamma)$.

Proof. We use the identity

$$\kappa(\tilde{\Sigma}_\dagger) = \|\tilde{\Sigma}_\dagger\|_2 \cdot \|\tilde{\Sigma}_\dagger^{-1}\|_2,$$

and bound $\|\tilde{\Sigma}_\dagger^{-1}\|_2$ by

$$\|\tilde{\Sigma}_\dagger^{-1}\|_2 = \frac{1}{\lambda_n^\dagger + \sigma^2} \leq \frac{1}{\sigma^2},$$

where λ_n^\dagger is the smallest eigenvalue of $(\Sigma - \Sigma_{mn}^T \Sigma_m^{-1} \Sigma_{mn}) \circ \mathbf{T}(\gamma) + \Sigma_{mn}^T \Sigma_m^{-1} \Sigma_{mn} > 0$.

Therefore, we obtain

$$\begin{aligned} \kappa(\tilde{\Sigma}_\dagger) &= \|\tilde{\Sigma}_\dagger\|_2 \cdot \|\tilde{\Sigma}_\dagger^{-1}\|_2 \leq \frac{1}{\sigma^2} \cdot \|\tilde{\Sigma}_\dagger\|_2 \\ &= \frac{1}{\sigma^2} \cdot \|(\Sigma - \Sigma_{mn}^T \Sigma_m^{-1} \Sigma_{mn}) \circ \mathbf{T}(\gamma) + \Sigma_{mn}^T \Sigma_m^{-1} \Sigma_{mn} + \sigma^2 I_n\|_2 \\ &\leq \frac{1}{\sigma^2} \cdot \|(\Sigma - \Sigma_{mn}^T \Sigma_m^{-1} \Sigma_{mn}) \circ \mathbf{T}(\gamma)\|_2 + \|\Sigma_{mn}^T \Sigma_m^{-1} \Sigma_{mn}\|_2 + \|\sigma^2 I_n\|_2 \\ &= \frac{1}{\sigma^2} \cdot \left(\|(\Sigma - \Sigma_{mn}^T \Sigma_m^{-1} \Sigma_{mn}) \circ \mathbf{T}(\gamma)\|_2 + \|\Sigma_{mn}^T \Sigma_m^{-1} \Sigma_{mn}\|_2 + \sigma^2\right) \\ &= \frac{1}{\sigma^2} \cdot \left(\|(\Sigma - \Sigma_{mn}^T \Sigma_m^{-1} \Sigma_{mn}) \circ \mathbf{T}(\gamma)\|_2 + \|\Sigma_{mn}^T \Sigma_m^{-1} \Sigma_{mn}\|_2\right) + 1, \end{aligned}$$

where we used the triangle inequality.

Since $(\Sigma - \Sigma_{mn}^T \Sigma_m^{-1} \Sigma_{mn})$ and $\mathbf{T}(\gamma)$ are symmetric and positive semidefinite matrices we can apply Theorem 5.3.4 in [Horn and Johnson \[1991\]](#) to obtain

$$\|(\Sigma - \Sigma_{mn}^T \Sigma_m^{-1} \Sigma_{mn}) \circ \mathbf{T}(\gamma)\|_2 \leq \|\Sigma - \Sigma_{mn}^T \Sigma_m^{-1} \Sigma_{mn}\|_2 \cdot \|\mathbf{T}(\gamma)\|_2.$$

By Lemma [F.1](#), we obtain

$$\|\Sigma - \Sigma_{mn}^T \Sigma_m^{-1} \Sigma_{mn}\|_2 \leq \mathcal{O}_P\left(\lambda_{m+1} + \frac{n}{\sqrt{m}} \cdot \sigma_1^2\right).$$

By using $\|\cdot\|_2 \leq \|\cdot\|_F$ and $\frac{1}{n} \cdot \sum_{i=1}^n \sum_{j: \mathbf{T}(\gamma)_{i,j} \neq 0} 1 = n_\gamma$, we obtain

$$\begin{aligned} \|\mathbf{T}(\gamma)\|_2 &\leq \|\mathbf{T}(\gamma)\|_F = \sqrt{\sum_{i=1}^n \sum_{j=1}^n |[\mathbf{T}(\gamma)]_{i,j}|^2} = \sqrt{\sum_{i=1}^n \sum_{j: \mathbf{T}(\gamma)_{i,j} \neq 0} |[\mathbf{T}(\gamma)]_{i,j}|^2} \\ &\leq \sqrt{\sum_{i=1}^n \sum_{j: \mathbf{T}(\gamma)_{i,j} \neq 0} 1} = \sqrt{n \cdot n_\gamma}. \end{aligned}$$

Moreover, using the Loewner order \preceq , see, e.g., Chapter 7 in [Jahn \[2020\]](#), we know that $0 \preceq (\Sigma - \Sigma_{mn}^T \Sigma_m^{-1} \Sigma_{mn})$ since $(\Sigma - \Sigma_{mn}^T \Sigma_m^{-1} \Sigma_{mn})$ is positive semidefinite and therefore, we have $\Sigma_{mn}^T \Sigma_m^{-1} \Sigma_{mn} \preceq \Sigma$ and obtain

$$\|\Sigma_{mn}^T \Sigma_m^{-1} \Sigma_{mn}\|_2 \leq \|\Sigma\|_2 = \lambda_1.$$

In conclusion, we obtain

$$\begin{aligned} \kappa(\tilde{\Sigma}_\dagger) &\leq \frac{1}{\sigma^2} \cdot \left(\|(\Sigma - \Sigma_{mn}^T \Sigma_m^{-1} \Sigma_{mn}) \circ \mathbf{T}(\gamma)\|_2 + \|\Sigma_{mn}^T \Sigma_m^{-1} \Sigma_{mn}\|_2 \right) + 1 \\ &\leq \mathcal{O}_P\left(\frac{1}{\sigma^2} \cdot \left(\left(\lambda_{m+1} + \frac{n}{\sqrt{m}} \cdot \sigma_1^2 \right) \cdot \sqrt{n \cdot n_\gamma} + \lambda_1 \right)\right) + 1. \end{aligned}$$

□

Proof of Theorem [3.2](#). We begin by stating a well-known CG convergence result [[Trefethen and Bau, 2022](#)], which bounds the error in terms of the conditioning number

$$\frac{\|\mathbf{u}^* - \mathbf{u}_k\|_{\tilde{\Sigma}_\dagger}}{\|\mathbf{u}^* - \mathbf{u}_0\|_{\tilde{\Sigma}_\dagger}} \leq 2 \cdot \left(\frac{\sqrt{\kappa(\tilde{\Sigma}_\dagger)} - 1}{\sqrt{\kappa(\tilde{\Sigma}_\dagger)} + 1} \right)^k.$$

By using Lemma F.2, we obtain

$$\begin{aligned}
\frac{\|\mathbf{u}^* - \mathbf{u}_k\|_{\tilde{\Sigma}_\dagger}}{\|\mathbf{u}^* - \mathbf{u}_0\|_{\tilde{\Sigma}_\dagger}} &\leq 2 \cdot \left(\frac{\sqrt{\kappa(\tilde{\Sigma}_\dagger) - 1}}{\sqrt{\kappa(\tilde{\Sigma}_\dagger) + 1}} \right)^k \\
&\leq 2 \cdot \left(\frac{\sqrt{\mathcal{O}_P\left(\frac{1}{\sigma^2} \cdot \left((\lambda_{m+1} + \frac{n}{\sqrt{m}} \cdot \sigma_1^2) \cdot \sqrt{n \cdot n_\gamma} + \lambda_1\right)\right) + 1 - 1}}{\sqrt{\mathcal{O}_P\left(\frac{1}{\sigma^2} \cdot \left((\lambda_{m+1} + \frac{n}{\sqrt{m}} \cdot \sigma_1^2) \cdot \sqrt{n \cdot n_\gamma} + \lambda_1\right)\right) + 1 + 1}} \right)^k \\
&\leq 2 \cdot \left(\frac{\sqrt{\mathcal{O}_P\left(\frac{1}{\sigma^2} \cdot \left((\lambda_{m+1} + \frac{n}{\sqrt{m}} \cdot \sigma_1^2) \cdot \sqrt{n \cdot n_\gamma} + \lambda_1\right)\right) + 1 - 1}}{\sqrt{\mathcal{O}_P\left(\frac{1}{\sigma^2} \cdot \left((\lambda_{m+1} + \frac{n}{\sqrt{m}} \cdot \sigma_1^2) \cdot \sqrt{n \cdot n_\gamma} + \lambda_1\right)\right) + 1}} \right)^k \\
&\leq 2 \cdot \left(\frac{1}{1 + \mathcal{O}_P\left(\sigma \cdot \left((\lambda_{m+1} + \frac{n}{\sqrt{m}} \cdot \sigma_1^2) \cdot \sqrt{n \cdot n_\gamma} + \lambda_1\right)^{-\frac{1}{2}}\right)} \right)^k.
\end{aligned}$$

□

Lemma F.3. Bound for the Condition Number of $\hat{\mathbf{P}}^{-1}\tilde{\Sigma}_\dagger$

Let $\tilde{\Sigma}_\dagger \in \mathbb{R}^{n \times n}$ be the FSA of a covariance matrix $\tilde{\Sigma} = \Sigma + \sigma^2 I_n \in \mathbb{R}^{n \times n}$ depending on the number of inducing points m and taper range γ , where Σ has eigenvalues $\lambda_1 \geq \dots \geq \lambda_n > 0$. Furthermore, let $\hat{\mathbf{P}} \in \mathbb{R}^{n \times n}$ be the FITC preconditioner for $\tilde{\Sigma}_\dagger$. Under Assumptions 1–3, the condition number $\kappa(\hat{\mathbf{P}}^{-1}\tilde{\Sigma}_\dagger)$ is bounded by

$$\kappa(\hat{\mathbf{P}}^{-1}\tilde{\Sigma}_\dagger) \leq \left(1 + \mathcal{O}_P\left(\frac{1}{\sigma^2} \cdot \left(\lambda_{m+1} + \frac{n}{\sqrt{m}} \cdot \sigma_1^2\right) \cdot \sqrt{n \cdot (n_\gamma - 1)}\right) \right)^2,$$

where n_γ is the average number of non-zero entries per row in $\mathbf{T}(\gamma)$.

Proof. For $\mathbf{E} = \tilde{\Sigma}_\dagger - \hat{\mathbf{P}}$, we obtain

$$\begin{aligned}
\kappa(\hat{\mathbf{P}}^{-1}\tilde{\Sigma}_\dagger) &= \|\hat{\mathbf{P}}^{-1}\tilde{\Sigma}_\dagger\|_2 \cdot \|\tilde{\Sigma}_\dagger^{-1}\hat{\mathbf{P}}\|_2 \\
&= \|\hat{\mathbf{P}}^{-1}(\hat{\mathbf{P}} + \mathbf{E})\|_2 \cdot \|\tilde{\Sigma}_\dagger^{-1}(\tilde{\Sigma}_\dagger - \mathbf{E})\|_2 \\
&= \|\mathbf{I}_n + \hat{\mathbf{P}}^{-1}\mathbf{E}\|_2 \cdot \|\mathbf{I}_n - \tilde{\Sigma}_\dagger^{-1}\mathbf{E}\|_2.
\end{aligned}$$

Applying Cauchy-Schwarz and the triangle inequality, we have

$$\kappa(\hat{\mathbf{P}}^{-1}\tilde{\Sigma}_\dagger) \leq (1 + \|\hat{\mathbf{P}}^{-1}\|_2 \cdot \|\mathbf{E}\|_2) \cdot (1 + \|\tilde{\Sigma}_\dagger^{-1}\|_2 \cdot \|\mathbf{E}\|_2).$$

Furthermore, similar to the first step in the proof of Lemma F.2, we have $\|\widehat{\mathbf{P}}^{-1}\|_2 \leq \frac{1}{\sigma^2}$ and $\|\tilde{\Sigma}_\dagger^{-1}\|_2 \leq \frac{1}{\sigma^2}$. Therefore, we obtain

$$\begin{aligned}\kappa(\widehat{\mathbf{P}}^{-1}\tilde{\Sigma}_\dagger) &\leq \left(1 + \frac{1}{\sigma^2} \cdot \|\mathbf{E}\|_2\right)^2 = \left(1 + \frac{1}{\sigma^2} \cdot \|\tilde{\Sigma}_s - \text{diag}(\tilde{\Sigma}_s)\|_2\right)^2 \\ &= \left(1 + \frac{1}{\sigma^2} \cdot \|(\Sigma - \Sigma_{mn}^T \Sigma_m^{-1} \Sigma_{mn}) \circ \mathbf{T}(\gamma) \right. \\ &\quad \left. - (\Sigma - \Sigma_{mn}^T \Sigma_m^{-1} \Sigma_{mn}) \circ \text{diag}(\mathbf{T}(\gamma))\|_2\right)^2 \\ &= \left(1 + \frac{1}{\sigma^2} \cdot \|(\Sigma - \Sigma_{mn}^T \Sigma_m^{-1} \Sigma_{mn}) \circ (\mathbf{T}(\gamma) - \text{diag}(\mathbf{T}(\gamma)))\|_2\right)^2.\end{aligned}$$

Since $(\Sigma - \Sigma_{mn}^T \Sigma_m^{-1} \Sigma_{mn})$ is positive semidefinite and symmetric and additionally $\mathbf{T}(\gamma) - \text{diag}(\mathbf{T}(\gamma))$ is symmetric we can apply Theorem 5.3.4 in [Horn and Johnson \[1991\]](#) to obtain

$$\begin{aligned}\kappa(\widehat{\mathbf{P}}^{-1}\tilde{\Sigma}_\dagger) &\leq \left(1 + \frac{1}{\sigma^2} \cdot \|(\Sigma - \Sigma_{mn}^T \Sigma_m^{-1} \Sigma_{mn}) \circ (\mathbf{T}(\gamma) - \text{diag}(\mathbf{T}(\gamma)))\|_2\right)^2 \\ &\leq \left(1 + \frac{1}{\sigma^2} \cdot \|\Sigma - \Sigma_{mn}^T \Sigma_m^{-1} \Sigma_{mn}\|_2 \cdot \|\mathbf{T}(\gamma) - \text{diag}(\mathbf{T}(\gamma))\|_2\right)^2.\end{aligned}$$

Moreover, using the same arguments as in the proof of Lemma F.2, we obtain

$$\kappa(\widehat{\mathbf{P}}^{-1}\tilde{\Sigma}_\dagger) \leq \left(1 + \mathcal{O}_P\left(\frac{1}{\sigma^2} \cdot (\lambda_{m+1} + \frac{n}{\sqrt{m}} \cdot \sigma_1^2) \cdot \sqrt{n \cdot (n_\gamma - 1)}\right)\right)^2.$$

□

Proof of Theorem 3.3. By proceeding analogue to the proof of Theorem 3.2 and by using Lemma F.3, we obtain

$$\begin{aligned}\frac{\|\mathbf{u}^* - \mathbf{u}_k\|_{\tilde{\Sigma}_\dagger}}{\|\mathbf{u}^* - \mathbf{u}_0\|_{\tilde{\Sigma}_\dagger}} &\leq 2 \cdot \left(\frac{\sqrt{\kappa(\widehat{\mathbf{P}}^{-1}\tilde{\Sigma}_\dagger) - 1}}{\sqrt{\kappa(\widehat{\mathbf{P}}^{-1}\tilde{\Sigma}_\dagger) + 1}}\right)^k \\ &\leq 2 \cdot \left(\frac{1 + \mathcal{O}_P\left(\frac{1}{\sigma^2} \cdot (\lambda_{m+1} + \frac{n}{\sqrt{m}} \cdot \sigma_1^2) \cdot \sqrt{n \cdot (n_\gamma - 1)}\right) - 1}{1 + \mathcal{O}_P\left(\frac{1}{\sigma^2} \cdot (\lambda_{m+1} + \frac{n}{\sqrt{m}} \cdot \sigma_1^2) \cdot \sqrt{n \cdot (n_\gamma - 1)}\right) + 1}\right)^k \\ &= 2 \cdot \left(\frac{\mathcal{O}_P\left(\frac{1}{\sigma^2} \cdot (\lambda_{m+1} + \frac{n}{\sqrt{m}} \cdot \sigma_1^2) \cdot \sqrt{n \cdot (n_\gamma - 1)}\right)}{\mathcal{O}_P\left(\frac{1}{\sigma^2} \cdot (\lambda_{m+1} + \frac{n}{\sqrt{m}} \cdot \sigma_1^2) \cdot \sqrt{n \cdot (n_\gamma - 1)}\right) + 2}\right)^k \\ &\leq 2 \cdot \left(\frac{1}{1 + \mathcal{O}_P\left(\sigma^2 \cdot ((\lambda_{m+1} + \frac{n}{\sqrt{m}} \cdot \sigma_1^2) \cdot \sqrt{n \cdot (n_\gamma - 1)})^{-1}\right)}\right)^k.\end{aligned}$$

□

G Choice of full-scale approximation parameters

In Figure 6, we report the negative log-likelihood evaluated at the data-generating parameters for different numbers of inducing points $m \in \{100, 200, \dots, 1'000\}$ and taper ranges $n_\gamma \in \{10, 20, \dots, 120\}$ when using the above-mentioned range parameters. As expected, in scenarios with a low effective range, characterized by minimal large-scale spatial dependence, the number of inducing points m has a small effect on the negative log-likelihood, and the residual process captures most of the dependence already with a relatively small range γ . Conversely, in cases with a large effective range, the FSA needs a large number of inducing points m , and the taper range γ is less important to achieve a good approximation. For our subsequent simulation studies, we use $m = 500$ and $\gamma = 0.016$ corresponding to $n_\gamma = 80$ as a reasonable balance between accuracy and computational efficiency.

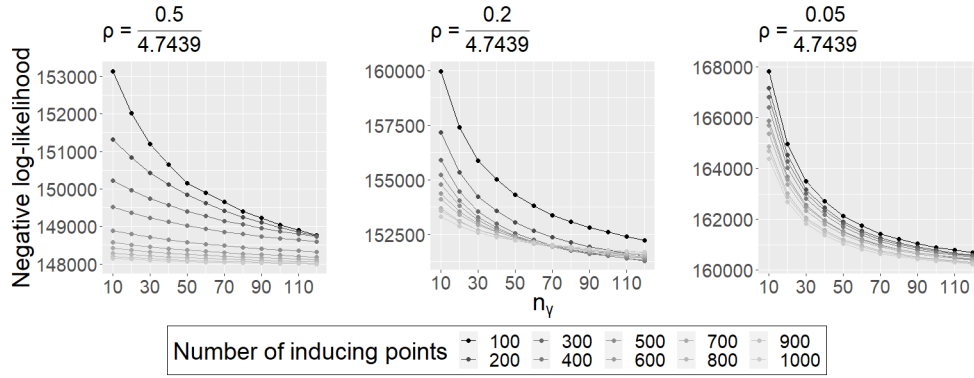


Figure 6: The negative log-likelihood for different combinations of the number of inducing points m and the taper range γ (n_γ) for different effective ranges (0.5, 0.2, 0.05 from left to right).

H Additional plots and tables

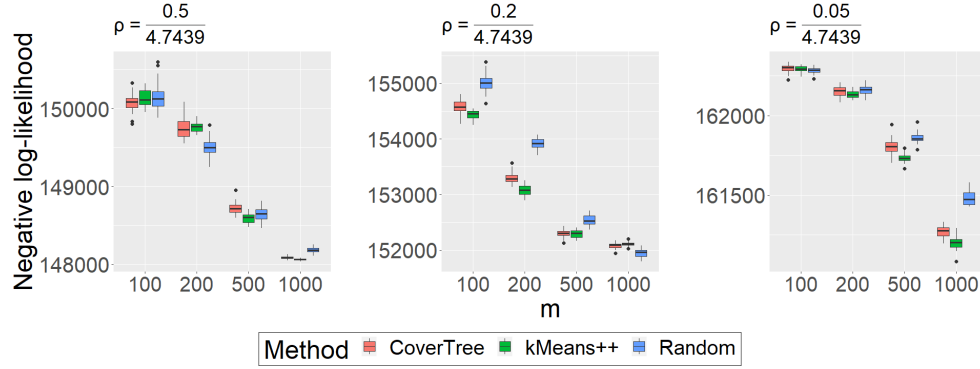


Figure 7: Box-plots of the negative log-likelihood for the FSA with $n_\gamma = 80$ for different effective ranges (0.5, 0.2, 0.05 from left to right) and numbers of inducing points m .

	Effective range 0.5		Effective range 0.2		Effective range 0.05	
	Lanczos	Stochastic	Lanczos	Stochastic	Lanczos	Stochastic
$k, \ell = 50$						
Log-Score	1.4716	1.4717 (1.7e-07)	1.4881	1.4875 (1.0e-05)	1.5964	1.5722 (4.8e-05)
RMSE	0.0018	9.4e-05 (2.4e-06)	0.066	0.0060 (2.0e-05)	0.56	0.047 (2.2e-05)
Time (s)	50	51	53	56	57	60
$k, \ell = 200$						
Log-Score	1.4716	1.4717 (7.4e-08)	1.4881	1.4875 (5.0e-06)	1.5960	1.5719 (5.9e-05)
RMSE	0.0015	3.0e-05 (5.0e-07)	0.0648	0.0028 (9.6e-06)	0.55	0.022 (7.2e-05)
Time (s)	53	57	57	60	60	64
$k, \ell = 500$						
Log-Score	1.4716	1.4717 (4.1e-08)	1.4880	1.4875 (3.5e-06)	1.5953	1.5719 (8.7e-06)
RMSE	0.0013	1.8e-05 (3.4e-07)	0.061	0.0018 (7.4e-06)	0.54	0.014 (1.3e-05)
Time (s)	62	63	67	67	72	72
$k, \ell = 1000$						
Log-Score	1.4716	1.4717 (2.8e-08)	1.4879	1.4875 (2.0e-06)	1.5942	1.5719 (6.6e-06)
RMSE	0.0011	1.3e-05 (1.8e-07)	0.056	0.0012 (3.8e-06)	0.53	0.010 (1.2e-10)
Time (s)	120	77	124	80	128	87
$k, \ell = 2000$						
Log-Score	1.4717	1.4717 (2.4e-08)	1.4877	1.4875 (1.5e-06)	1.5922	1.5719 (7.9e-06)
RMSE	0.00086	9.1e-06 (2.1e-07)	0.0470	0.00087 (2.4e-06)	0.50	0.0071 (1.4e-05)
Time (s)	405	122	409	126	413	131
$k, \ell = 5000$						
Log-Score	1.4717	1.4717 (9.9e-09)	1.4875	1.4875 (8.7e-07)	1.5869	1.5718 (5.8e-06)
RMSE	0.00044	6.0e-06 (1.2e-07)	0.028	0.00055 (1.9e-06)	0.42	0.0045 (2.6e-06)
Time (s)	1452	198	1453	203	1468	210
Cholesky:						
Log-Score	1.4717		1.4875		1.5718	
Time (s)	1651		1652		1658	

Table 3: Log-Score and RMSE of the predictive variance approximation computed by using the Cholesky factor, Lanczos methods and stochastic diagonal approximations with different ranks k and number of sample vectors ℓ . In the case of stochastic computations, we report the mean and standard deviation for the Log-Score and RMSE.

		Effective range 0.5		Effective range 0.2		Effective range 0.05	
		Cholesky	Iterative	Cholesky	Iterative	Cholesky	Iterative
Parameter Estimation	Bias of σ^2	0.0211	0.0215	0.0321	0.0327	0.0135	0.0147
	RMSE	0.0218	0.0222	0.0325	0.0330	0.0146	0.0157
	Bias of σ_1^2	0.0905	0.0519	0.0782	0.0808	0.0356	0.0344
	RMSE	0.161	0.222	0.161	0.162	0.0394	0.0384
	Bias of ρ	0.0629	0.0624	0.0106	0.0107	0.00346	0.00341
	RMSE	0.0630	0.0625	0.0109	0.0109	0.00348	0.00343
	Speed-up	8.2		7.5		6.3	
Prediction	RMSE	1.0374	1.0374	1.0673	1.0673	1.1515	1.1516
	SE	0.00047	0.00047	0.00068	0.00069	0.0010	0.0010
	Log-Score	1.4559	1.4559	1.4847	1.4847	1.5605	1.5605
	SE	0.00044	0.00044	0.00063	0.00063	0.00089	0.00089
	CRPS	0.5854	0.5854	0.6023	0.6023	0.6498	0.6499
	SE	0.00024	0.00024	0.00039	0.00039	0.00059	0.00059
	Speed-up	32.4		27.2		22.6	
Total speed-up		11.6		11.2		8.9	

Table 4: Bias and RMSE of the estimated covariance parameters over 10 simulation runs and the averages and standard errors (SE) of the predictive measures (RMSE, log-score, CRPS) and the average speed-up between the iterative method with the FITC preconditioner and the Cholesky-based computations.

I Simulation study

I.1 Negative log-likelihood

I.1.1 Accuracy

In Figures 8 - 10, we show the relative error in the negative log-likelihood calculated with our iterative methods compared to Cholesky-based calculations on simulated random fields with effective range 0.05, 0.2 and 0.5, respectively, for the true population parameters and for a relatively simple choice of initial values computed as $\sigma^2 = \sigma_1^2 = \text{Var}(\mathbf{y})/2$ and $\rho = \frac{\sqrt{3}}{4.7 \cdot m^2} \sum_{i=1}^m \sum_{j=1}^m \|\mathbf{s}_i^* - \mathbf{s}_j^*\|_2$, the latter corresponds to an effective range of the average distance among the inducing points. We consider both the FITC preconditioner and the CG method without a preconditioner. We observe only minor deviations between the Cholesky and iterative methods-based log-likelihoods, and the preconditioner results in variance reduction. Concerning the latter, we find that the range parameter influences the amount of variance reduction. We have also compared Rademacher-distributed and normally-distributed sample vectors, but no significant differences in the stochastic estimates were evident (results not tabulated).

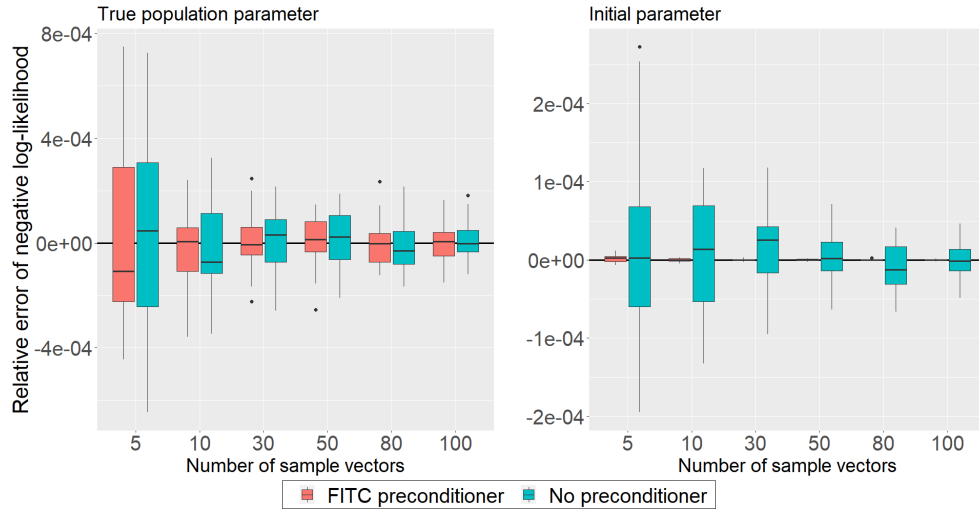


Figure 8: Box-plots of the relative error of the negative log-likelihood computed with and without the FITC preconditioner on a simulated random field with an effective range of 0.05 for the true population parameters $\sigma^2 = 1$, $\sigma_1^2 = 1$ and $\rho = \frac{0.05}{4.7439}$ (left) and the initial parameters $\sigma^2 = 0.99673$, $\sigma_1^2 = 0.99673$ and $\rho = 0.192256$ (right).

I.2 Comparison of preconditioners

In Table 5, we observe that the CG method needs fewer iterations when the effective range is smaller. This observation aligns with the outcomes detailed in Theorem 3.2, as a diminished range parameter corresponds to a reduced largest eigenvalue of Σ . For larger effective ranges, all preconditioners accelerate the convergence of the CG method.

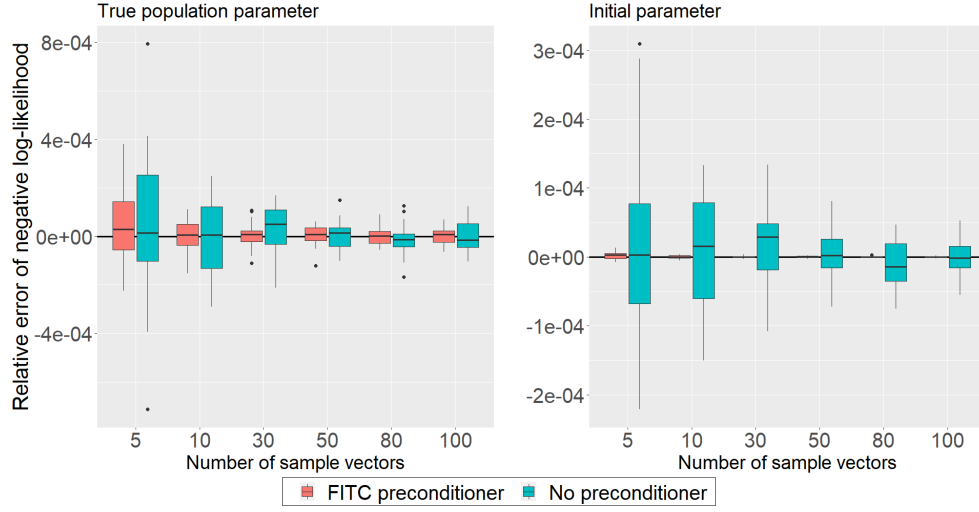


Figure 9: Box-plots of the relative error of the negative log-likelihood computed with and without the FITC preconditioner on a simulated random field with an effective range of 0.2 for the true population parameters $\sigma^2 = 1$, $\sigma_1^2 = 1$ and $\rho = \frac{0.2}{4.7439}$ (left) and the initial parameters $\sigma^2 = 0.99673$, $\sigma_1^2 = 0.99673$ and $\rho = 0.192256$ (right).

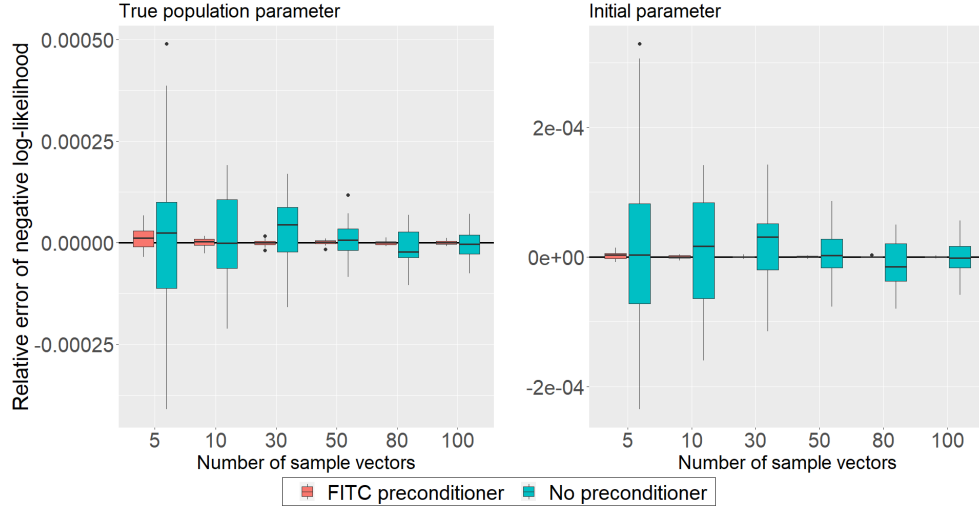


Figure 10: Box-plots of the relative error of the negative log-likelihood computed with and without the FITC preconditioner on a simulated random field with an effective range of 0.5 for the true population parameters $\sigma^2 = 1$, $\sigma_1^2 = 1$ and $\rho = \frac{0.5}{4.7439}$ (left) and the initial parameters $\sigma^2 = 0.99673$, $\sigma_1^2 = 0.99673$ and $\rho = 0.192256$ (right).

Effective Range	0.5	0.2	0.05
No preconditioner			
CG-Iterations for $\tilde{\Sigma}_{\dagger}^{-1} \mathbf{y}$	312	190	44
Time for computing negative log-likelihood (s)	94	54	14
FITC preconditioner			
CG-Iterations for $\tilde{\Sigma}_{\dagger}^{-1} \mathbf{y}$	7	14	24
Time for computing negative log-likelihood (s)	7	10	15
Pivoted Cholesky ($k = 200$)			
CG-Iterations for $\tilde{\Sigma}_{\dagger}^{-1} \mathbf{y}$	47	91	44
Time for computing negative log-likelihood (s)	35	52	33
Pivoted Cholesky ($k = 500$)			
CG-Iterations for $\tilde{\Sigma}_{\dagger}^{-1} \mathbf{y}$	26	52	43
Time for computing negative log-likelihood (s)	70	83	80
Pivoted Cholesky ($k = 1'000$)			
CG-Iterations for $\tilde{\Sigma}_{\dagger}^{-1} \mathbf{y}$	13	32	42
Time for computing negative log-likelihood (s)	243	266	273

Table 5: Number of (preconditioned) CG-iterations for the linear solve $\tilde{\Sigma}_{\dagger}^{-1} \mathbf{y}$ and the time in seconds (s) for computing the negative log-likelihood for the true population parameters.

I.3 Gradient of negative log-likelihood

Next, we analyze the accuracy of the stochastic approximations of the derivatives of the negative log-likelihood. We consider the relative error of iterative methods compared to Cholesky-based calculations. This analysis is carried out for the true population parameters on simulated random fields with an effective range 0.05, 0.2 and 0.5, respectively. For the iterative methods, we consider three distinct approaches: employing no preconditioner as well as using the FITC preconditioner and variance reduction techniques with $\hat{c}_{\text{opt}} = 1$ and \hat{c}_{opt} as outlined in (10). Figures 11-13 show the results. The FITC preconditioner method results in lower variance, with a slight further reduction observed when employing the optimal parameter \hat{c}_{opt} .

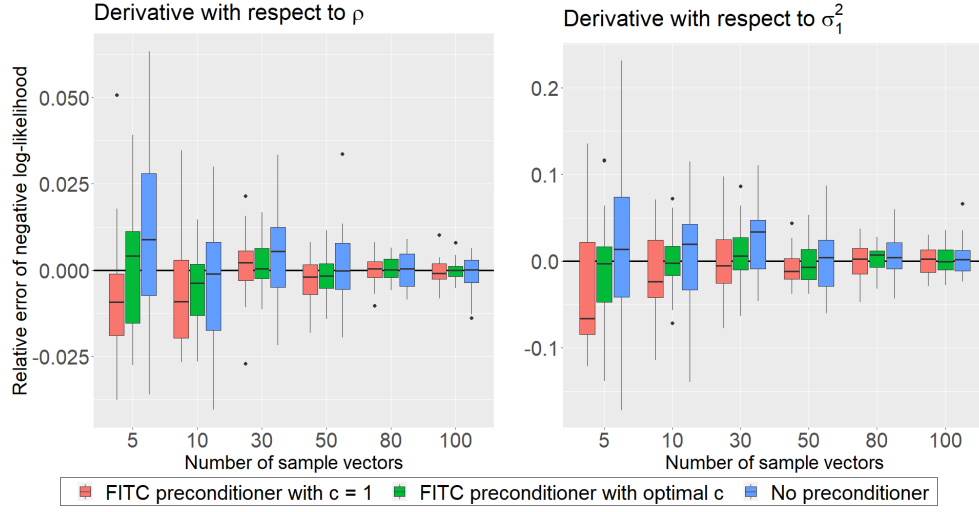


Figure 11: Box-plots of the relative error of the derivatives of the negative log-likelihood computed without a preconditioner, with the FITC-preconditioner and additionally with estimating \hat{c}_{opt} for an effective range of 0.05 and the true population parameters.

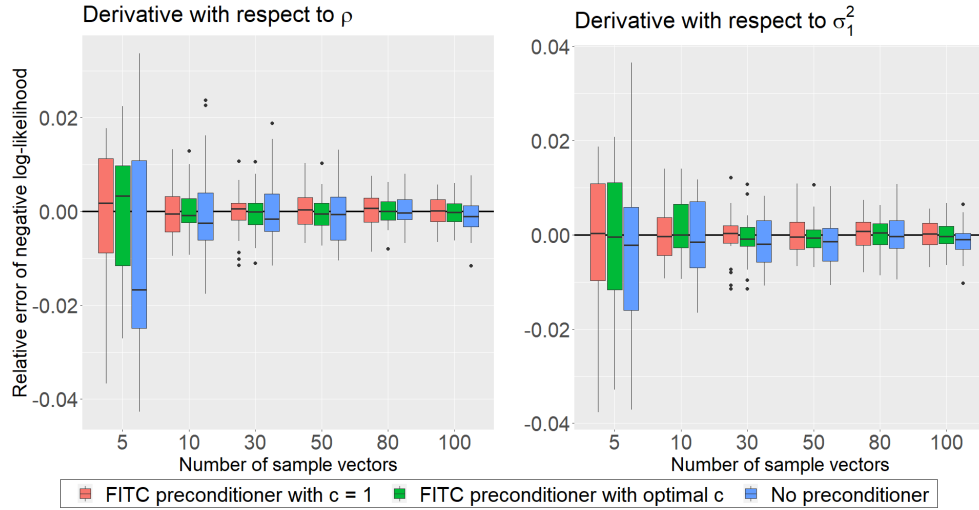


Figure 12: Box-plots of the relative error of the derivatives of the negative log-likelihood computed without a preconditioner, with the FITC-preconditioner and additionally with estimating \hat{c}_{opt} for an effective range of 0.2 and the true population parameters.

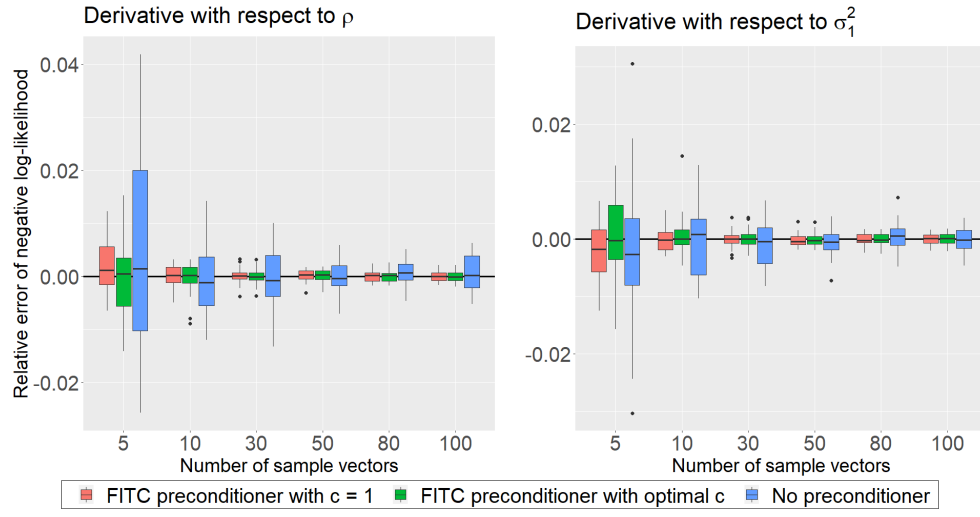


Figure 13: Box-plots of the relative error of the derivatives of the negative log-likelihood computed without a preconditioner, with the FITC-preconditioner and additionally with estimating \hat{c}_{opt} for an effective range of 0.5 and the true population parameters.

J Real-world application

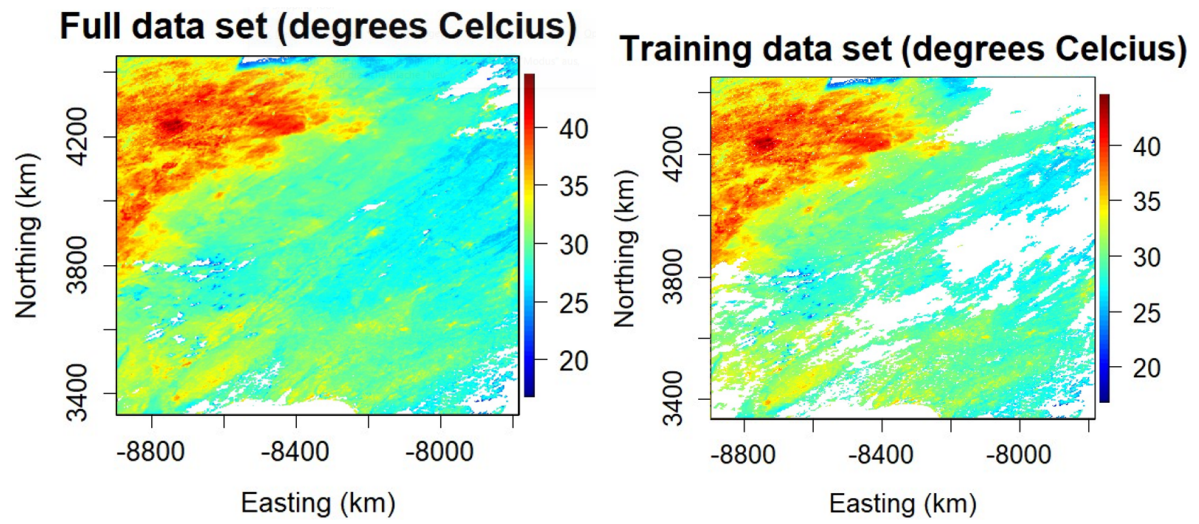


Figure 14: The full (left) and training (right) satellite data set.

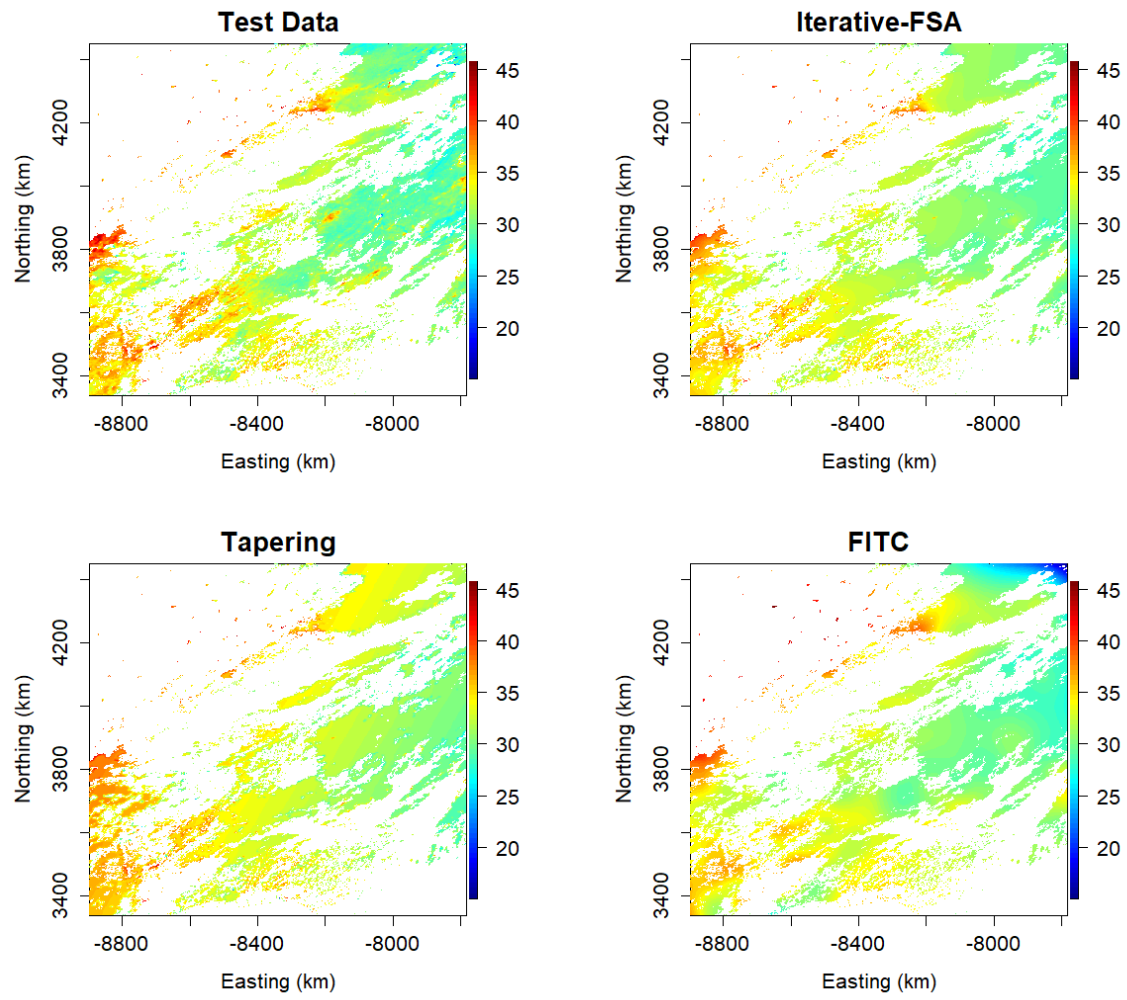


Figure 15: Test data and predictive means in the FSA (iterative), tapering, and FITC framework.

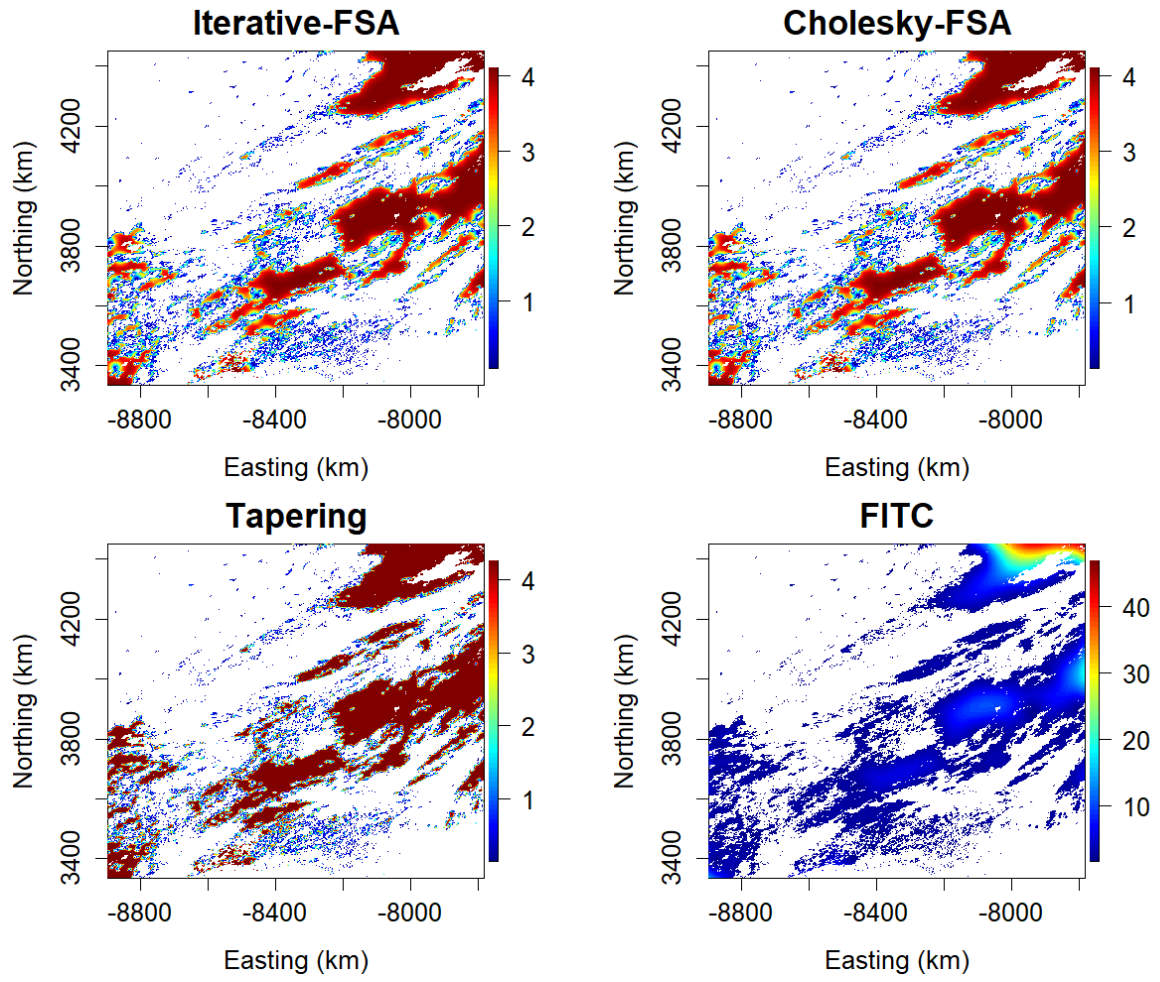


Figure 16: Predictive variances in the FSA (iterative and Cholesky-based), tapering, and FITC framework.

	FSA		Tapering	FITC
	Iterative	Cholesky	Cholesky	Cholesky
Estimation:				
$\beta_{\text{intercept}}$	-26.30	-26.18	-48.32	61.51
β_{east}	-0.006602	-0.006590	-0.007599	-0.01995
β_{north}	0.0009043	0.0008980	0.004841	-0.05131
σ^2	0.1428	0.1429	0.01968	1.909
σ_1^2	4.093	4.099	4.527	111.1
ρ	24.13	24.16	5.494	211.1
Time (s)	5054	33212	13086	12445
Speed-up	6.6		2.5	2.7
Prediction:				
RMSE	1.4177	1.4175	2.3349	1.8171
Log-Score	1.7244	1.7245	2.1735	1.9444
CRPS	0.75451	0.75449	1.2723	0.94036
Time (s)	587	5513	199	67.55
Speed-up	9.4		27.8	81.6
Total:				
Time (s)	5641	38725	13285	12512
Speed-up	6.9		2.9	3.1

Table 6: Real-world satellite data results.

δ	0.001		1		10	
ℓ	50	20	50	20	50	20
Estimation						
$\beta_{\text{intercept}}$	-26.16	-26.15	-26.30	-26.42	-26.57	-27.87
β_{east}	-0.006586	-0.006586	-0.006602	-0.006612	-0.006645	-0.006705
β_{north}	0.0009011	0.0008971	0.0009043	0.0009117	0.0008818	0.0001101
σ^2	0.1428	0.1428	0.1428	0.1427	0.1424	0.1434
σ_1^2	4.103	4.105	4.093	4.091	4.079	4.0328
ρ	24.16	24.17	24.13	24.10	24.03	23.96
Time (s)	7678	5753	5054	3782	4668	3513
Speed-up	4.3	5.8	6.6	8.8	7.11	9.5
Prediction						
RMSE	1.4175	1.4174	1.4177	1.4173	1.4169	1.4250
Log-Score	1.7246	1.7246	1.7244	1.7242	1.7236	1.7252
CRPS	0.75450	0.75450	0.75450	0.75423	0.75400	0.75734
Time (s)	1628	1630	587	592	392	390
Speed-up	3.4	3.4	9.4	9.3	14.1	14.16
Total						
Time (s)	9306	7383	5641	4374	5060	3903
Speed-up	4.2	5.3	6.9	8.9	7.7	9.9

Table 7: Results for GP inference using the iterative method with the FITC preconditioner with different CG convergence tolerances $\delta \in \{0.001, 1, 10\}$ and numbers of sample vectors $\ell \in \{50, 20\}$.

References

- D. Arthur and S. Vassilvitskii. K-means++ the advantages of careful seeding. In *Proceedings of the eighteenth annual ACM-SIAM symposium on Discrete algorithms*, pages 1027–1035, 2007.
- E. Aune, D. P. Simpson, and J. Eidsvik. Parameter estimation in high dimensional gaussian distributions. *Statistics and Computing*, 24:247–263, 2014.
- S. Banerjee, A. E. Gelfand, A. O. Finley, and H. Sang. Gaussian predictive process models for large spatial data sets. *Journal of the Royal Statistical Society Series B: Statistical Methodology*, 70(4):825–848, 2008.
- C. Bekas, E. Kokiopoulou, and Y. Saad. An estimator for the diagonal of a matrix. *Applied numerical mathematics*, 57(11-12):1214–1229, 2007.
- T. A. Davis. *Direct methods for sparse linear systems*. SIAM, 2006.
- K. Dong, D. Eriksson, H. Nickisch, D. Bindel, and A. G. Wilson. Scalable log determinants for gaussian process kernel learning. *Advances in Neural Information Processing Systems*, 30, 2017.
- C. Eckart and G. Young. The approximation of one matrix by another of lower rank. *Psychometrika*, 1(3):211–218, 1936.
- A. O. Finley, H. Sang, S. Banerjee, and A. E. Gelfand. Improving the performance of predictive process modeling for large datasets. *Computational statistics & data analysis*, 53(8):2873–2884, 2009.
- R. Furrer, M. G. Genton, and D. Nychka. Covariance tapering for interpolation of large spatial datasets. *Journal of Computational and Graphical Statistics*, 15(3):502–523, 2006.
- J. Gardner, G. Pleiss, K. Q. Weinberger, D. Bindel, and A. G. Wilson. Gpytorch: Blackbox matrix-matrix gaussian process inference with gpu acceleration. *Advances in neural information processing systems*, 31, 2018.
- M. J. Heaton, A. Datta, A. O. Finley, R. Furrer, J. Guinness, R. Guhaniyogi, F. Gerber, R. B. Gramacy, D. Hammerling, M. Katzfuss, et al. A case study competition among methods for analyzing large spatial data. *Journal of Agricultural, Biological and Environmental Statistics*, 24:398–425, 2019.
- R. A. Horn and C. R. Johnson. *Topics in matrix analysis* cambridge university press. Cambridge, UK, 1991.
- M. F. Hutchinson. A stochastic estimator of the trace of the influence matrix for laplacian smoothing splines. *Communications in Statistics-Simulation and Computation*, 18(3):1059–1076, 1989.
- J. Jahn. *Introduction to the theory of nonlinear optimization*. Springer Nature, 2020.

- S. Kumar, M. Mohri, and A. Talwalkar. Sampling methods for the nyström method. *The Journal of Machine Learning Research*, 13(1):981–1006, 2012.
- R. J. Lipton, D. J. Rose, and R. E. Tarjan. Generalized nested dissection. *SIAM journal on numerical analysis*, 16(2):346–358, 1979.
- W. J. Maddox, S. Kapoor, and A. G. Wilson. When are iterative gaussian processes reliably accurate? *arXiv preprint arXiv:2112.15246*, 2021.
- G. Pleiss, J. Gardner, K. Weinberger, and A. G. Wilson. Constant-time predictive distributions for gaussian processes. In *International Conference on Machine Learning*, pages 4114–4123. PMLR, 2018.
- J. Quinonero-Candela and C. E. Rasmussen. A unifying view of sparse approximate gaussian process regression. *The Journal of Machine Learning Research*, 6:1939–1959, 2005.
- H. Sang and J. Z. Huang. A full scale approximation of covariance functions for large spatial data sets. *Journal of the Royal Statistical Society Series B: Statistical Methodology*, 74(1):111–132, 2012.
- F. Sigrist. Gaussian process boosting. *The Journal of Machine Learning Research*, 23(1):10565–10610, 2022a.
- F. Sigrist. Latent gaussian model boosting. *IEEE Transactions on Pattern Analysis and Machine Intelligence*, 45(2):1894–1905, 2022b.
- J. J. Sylvester. Xxxvii. on the relation between the minor determinants of linearly equivalent quadratic functions. *The London, Edinburgh, and Dublin Philosophical Magazine and Journal of Science*, 1(4):295–305, 1851.
- A. Terenin, D. R. Burt, A. Artemev, S. Flaxman, M. van der Wilk, C. E. Rasmussen, and H. Ge. Numerically stable sparse gaussian processes via minimum separation using cover trees. *arXiv preprint arXiv:2210.07893*, 2022.
- L. N. Trefethen and D. Bau. *Numerical linear algebra*, volume 181. Siam, 2022.
- S. Ubaru, J. Chen, and Y. Saad. Fast estimation of $\text{tr}(f(a))$ via stochastic lanczos quadrature. *SIAM Journal on Matrix Analysis and Applications*, 38(4):1075–1099, 2017.
- M. A. Woodbury. *Inverting modified matrices*. Department of Statistics, Princeton University, 1950.